The Dissertation Committee for Maria Elizabeth Bell
certifies that this is the approved version of the following dissertation:

Vesicle-free transition zones, dense core vesicles, and vesicle pool redistribution contribute to synapse growth following LTP induction

Committee:

_____

Kristen Harris, Supervisor

_____

Richard Aldrich

_____

Deanna Benson

_____

Theresa Jones

_____

Hiroshi Nishiyama

Vesicle-free transition zones, dense core vesicles, and vesicle pool redistribution contribute to synapse growth following LTP induction

by

Maria Elizabeth Bell, B.A.; M.A.

Dissertation

Presented to the Faculty of the Graduate School of

The University of Texas at Austin

in Partial Fulfillment

of the Requirements

for the Degree of

Doctor of Philosophy

The University of Texas at Austin

May, 2012

Vesicle-free transition zones, dense core vesicles, and vesicle pool redistribution contribute to synapse growth following LTP induction

Maria Elizabeth Bell, Ph.D.

The University of Texas at Austin, 2012

Supervisor: Kristen Harris

Long-term potentiation (LTP) is a widely studied cellular mechanism of learning and memory. LTP occurs at excitatory synapses on dendritic spines. Two hours after LTP induction in mature rat hippocampal slices, a reduction in spine number that is perfectly balanced by enlargement of the remaining synapses was previously observed. The sequence of events by which mature synapses enlarge is not well understood, but potential pre- and postsynaptic ultrastructural correlates of synapse growth have been identified. Vesicle-free transition zones (VFTZs) are postsynaptic thickenings contiguous with the PSD that have no apposing presynaptic vesicles perpendicular to the presynaptic membrane. VFTZs could be regions where synapses have expanded postsynaptically, but to which presynaptic vesicles have not yet been recruited. Presynaptic 80-nm dense core vesicles (DCVs) transport active zone proteins to the synapse during synaptogenesis, and may perform the same function during synaptic plasticity. 3-D reconstructions from ssTEM were used to investigate changes in VFTZs, DCVs, and presynaptic vesicles following LTP induction. By 30 minutes, VFTZ area and docked vesicle count decreased, suggesting

mobilization of additional vesicles to the synapse and enhanced release or delayed recycling. By two hours, VFTZs enlarged, suggesting VFTZ assembly contributes to synapse enlargement. DCV count at 2 hours decreased relative to that at 30 minutes in both control and LTP conditions, suggesting DCVs were inserted at existing synapses to enlarge potentiated synapses in the LTP condition and to support ongoing spinogenesis in the control condition. The overall vesicle count in presynaptic boutons decreased at 2 hours following LTP induction, but docked vesicle count did not. Docked vesicle count was elevated at 2 hours relative to 30 minutes, suggesting that the depletion of docked vesicles observed at 30 minutes was followed by a replenishment and enhancement by 2 hours supplied by the non-docked vesicle pool. That the largest spines had more and larger VFTZs and recruited more DCVs and docked vesicles, and that the ratio of the sum of VFTZ area to the sum of PSD area is constant, provide further evidence that dendritic segments serve as functional units that manage resources in a coordinated and homeostatic way.

Table of Contents

Chapter 1

Introduction

In order to understand the underlying mechanisms of learning and memory, we study the brain at different levels, from the behavior that we exhibit down to the molecules of which the brain is composed. This work is focused on the synapse, the point of contact that facilitates the transfer of information from one cell to another. Specifically, this study explores how changes in synaptic structure correlate with changes in function, and what synaptic substructure informs us about what synaptic molecules may be driving these changes.

Most excitatory synapses occur on spines that protrude from neuronal dendrites. Mature dendrites are densely studded with these protrusions, and both spines and synapses vary in size and shape. Synapses are assembled and disassembled in response to various environmental stimuli and conditions throughout the life of a neuron, but not a lot is known about the subcellular sequence of events that occur at mature synapses undergoing synaptic remodeling. Previous work has uncovered a model system in which to study this process.

Long term potentiation (LTP) is a well characterized cellular mechanism of learning and memory that induces structural synaptic plasticity (Harris and Stevens, 1988,1989;Bliss and Collingridge, 1993;Yuste and Bonhoeffer, 2001;Bourne and Harris, 2008). Spine size increases following LTP induction (Lang et al., 2004;Matsuzaki et al., 2004;Nagerl et al., 2004;Ostroff et al., 2002), and spine volume correlates with the size of the PSD and the number of postsynaptic AMPA receptors (Hering and Sheng, 2001;Luscher et al., 2000;Matsuzaki et al., 2001;Matsuzaki et al., 2004). Electron microscopy (EM) in the mature dentate gyrus of the hippocampus has demonstrated modification of

synapse number and morphology within an hour after tetanic stimulation of the perforant pathway (Fifkova and Van Harreveld, 1977;Fifkova and Anderson, 1981;Desmond and Levy, 1983;Desmond and Levy, 1986a;Desmond and Levy, 1986b;Trommald et al., 1990;Geinisman et al., 1991;Geinisman et al., 1993;Trommald et al., 1996), which was accompanied by an enlargement of spines and synapses that persisted for several hours (Fifkova and Van Harreveld, 1977;Popov et al., 2004). More recently, it was demonstrated that LTP induction resulted in the loss of small spines, which was perfectly balanced by the enlargement of synapses on remaining spines in mature rat hippocampal CA1 (Bourne and Harris, 2011a). LTP induction in mature rat hippocampal CA1 therefore provides an ideal model system in which to study the question of how synapses enlarge by examining synaptic substructure. This study investigates the role of the vesicle-free transition zone (VFTZ) in postsynaptic enlargement during synaptic plasticity.

The process of synaptic enlargement in mature brain is not yet well understood. Clearly synaptic growth requires the trafficking of receptors and other postsynaptic proteins that form the postsynaptic density, the assembly of presynaptic active zone machinery to tether and release vesicles, pre- and postsynaptic transmembrane cell adhesion molecules to anchor the cells and provide bidirectional signaling, and the recruitment of additional presynaptic vesicles to increase neurotransmitter release. While synaptic plasticity studies in mature brain have shed some light on these processes, much of what we know about synapse growth comes from work in developing cortex.

Most excitatory synapses in adult brain are asymmetric junctions composed of a presynaptic terminal and a postsynaptic density and are located on dendritic spine heads (Harris and Kater, 1994). During development, before spines are expressed, cortical dendrites exhibit longer, thinner processes known as filopodia (Purpura, 1975), which are replaced by spines as the cortex matures. Filopodia have been shown to remain active along the lengths of dendrites in

hippocampal area CA1 during the initial 1–2 weeks in culture (Papa et al., 1995;Ziv and Smith, 1996). These filopodia are transient structures that can extend and retract in as little as10 minutes (Papa et al., 1995;Ziv and Smith, 1996). Electron micrographs (EMs) demonstrated that dendritic filopodia at 1 week in culture had no synaptic contacts (Papa et al., 1995). Both these and CA1 hippocampal slice experiments (Dailey and Smith, 1996;Collin et al., 1997) demonstrated a transition from a relatively small number of labile filopodial protrusions to a dense population of stable, adult-like spines over a roughly 4 week period.

Axo-dendritic synapses occur at points of contact between presynaptic axons and postsynaptic dendrites. The axonal presynaptic terminal contains hundreds of small (∼50 nm) synaptic vesicles (SSVs) that contain glutamate. Action potentials cause these vesicles to fuse with the presynaptic plasma membrane at specific locations known as presynaptic active zones (Burns et al., 1995;Phillips et al., 2001), releasing glutamate into the 20- 25 nm wide synaptic cleft (Schikorski and Stevens, 1997). The glutamate diffuses through the cleft and binds to glutamate-ligated N-methyl-D-aspartic acid (NMDA) and α-Amino-3-hydroxy-5-methyl-4-isoxazole proprionic acid (AMPA) receptors (NMDARs and AMPARs; Hollmann and Heinemann, 1994). These receptors are located in the postsynaptic density (PSD), an electron-dense structure composed of many proteins that is located opposite the presynaptic active zone in the dendritic spine (Kennedy, 2000). Activation of these receptors leads to an influx of ions, local depolarization, and activation of voltage-gated ion channels, among other processes. In order to build a synapse, glutamate receptors, PSD scaffolding proteins, cell adhesion molecules, presynaptic active zone proteins, and SSVs must be recruited to sites of physical contact between axons and dendrites in the appropriate sequence.

During synaptogenesis in young neurons, presynaptic proteins are transported to the synapse in both 80 nm dense core vesicles (DCVs) and

synaptic vesicle protein transport vesicles (SVTs; McAllister, 2007). DCVs transport such active zone proteins as piccolo and bassoon, while STVs contain the vesicular glutamate transport (vGlut1) and may therefore be capable of releasing glutamate along growing axons prior to synapse formation (Zhai et al., 2001;Sabo et al., 2006). DCVs also carry other active zone proteins that have been implicated in synaptic vesicle exocytosis, such as Munc13, Munc18, syntaxin, Snap25 and N-type calcium channels (Shapira et al., 2003;Zhai et al.,2001), and perhaps α-liprin133 and ERC (ELKS, Rab6-interacting protein 2 and CAST) (Ohtsuka et al., 2002), which have been implicated in linking active zone cytoskeletal matrix components together. The contents of 2–5 DCVs can account for the piccolo or bassoon content of a mature synapse (Bresler et al., 2004;Shapira et al., 2003), suggesting that presynaptic sites may be formed in a unitary fashion by the insertion of a number of quantal packets into the plasma membrane.

There is debate over whether most postsynaptic proteins are similarly transported in compact units or diffuse through the cytoplasm (Bresler et al., 2001;Friedman et al., 2000;Marrs et al., 2001;Okabe S et al., 1999;Rao et al., 1998;Sans et al., 2000;Washbourne et al., 2002) to reach the site of contact, but it has been shown that some NMDARs and AMPARs are transported within dendrites in discrete transport packets (Sans et al., 2003;Washbourne et al., 2004). NMDAR transport packets cycle with the plasma membrane during pauses in their trafficking during development (Washbourne et al., 2004), suggesting that they may detect glutamate. Excitatory synapse formation does not require glutamate release (Craig et al., 1994;Harms and Craig, 2005;Varoqueaux et al., 2002;Verhage et al., 2000), but without it the number of synapses formed decreased substantially (Bouwman et al., 2004), suggesting that this type of cycling may aid in initiating contact between axons and dendrites.

Synaptogenesis may occur at specific sites in response to a number of signals. First, sites of synapse formation coincide with sites where STVs pause and cycle with the axonal membrane, suggesting that filopodia may extend towards sites of glutamate release (Lohmann et al., 2005;Tashiro et al., 2003). Second, presynaptic terminals may form at stable sites of PSD-protein complexes. Therefore, predefined sites within axons and dendrites may determine where synapses can form along those processes. The time-course of synaptogenesis depends upon the stable accumulation of both “core components” of the glutamatergic synapse: presynaptic vesicles and postsynaptic glutamate receptors. Initial studies indicated that synapse formation takes days to weeks (Rao et al., 1998), but later time-lapse imaging studies have shown that synapse formation occurs within minutes (Friedman et al., 2000). Presynaptic proteins were shown to accumulate at stable sites of FM-64-labeled SSVs within 1-2 hours of SSV recruitment (Friedman et al., 2000; Ahmari and Smith, 2002), indicating that STVs are recruited with or slightly before DCVs. Other studies have demonstrated that the recruitment of postsynaptic proteins precedes the recruitment of presynaptic proteins to new synapses. Stable complexes of postsynaptic proteins PSD-95, GKAP, Shank, and neuroligin were observed at sites to which STVs congregated within 2 hours of postsynaptic complex formation (Gerrow et al., 2006). Together, these results suggest that there are multiple pre- and postsynaptic signaling pathways that work in parallel to form and stabilize nascent synapses.

Cell adhesion molecules (CAMs) appear to enable the initial formation of contacts between axons and dendrites. This class of molecule includes cadherins, integrins, and members of the immunoglobulin (Ig) superfamilies including sidekicks, NCAM, nectins, neuroligins, SynCAMs, SALMs, neuronal pentraxins, and ephrins (Akins and Biederer, 2006;Scheiffele, 2003;Waites et al., 2005), many of which are found pre- and/or postsynaptically at mature synapses (Scheiffele, 2003;Li and Sheng, 2003;Passafaro et al., 2003;Dityatev et al.,

2004;Sytnyk et al., 2004;Ziv and Garner, 2004). CAMs are capable of simultaneous bidirectional signaling between axon and dendrite, and can therefore coordinate rapid and concomitant pre- and postsynaptic protein recruitment (Washbourne et al., 2002) in order to contribute to synapse maintenance and synaptic plasticity (Li and Sheng, 2003). A few of these families have distinct characteristics that suggest each may have a direct role in synapse enlargement.

One such CAM family is the cadherins. Cadherins are heterotypic (they bind to each other across the synaptic cleft) and signal through binding to α- and β-catenins, which in turn bind to the actin cytoskeleton (Daniels et al., 2001;Ivanov et al., 2001). N-cadherin is transported along with active zone components to synaptogenic sites (Jontes et al., 2004;Shapira et al., 2003;Zhai et al., 2001). Cadherins rapidly appear at developing synapses (Benson and Tanaka, 1998), and excitatory synapse number (in developing and mature synapses) decreases when a dominant-negative form of N-cadherin is introduced (Togashi et al., 2002;Bozdagi et al., 2004), suggesting that cadherin-based adhesion stabilizes transient, labile contacts long enough to allow for the activation of signaling cascades that recruit other essential synaptic proteins (Togashi et al., 2002;Ziv and Garner, 2004). In addition, modifying N-cadherin function in young hippocampal cultures causes a dispersal of synapsin (Ziv and Garner, 2004;Togashi et al., 2002) and interfering with β-catenin alters the clustering of SSV proteins (Bamji et al., 2003), suggesting that the recruitment of SSVs to new synapses is dependent on cadherin/β-catenin signaling.

Though similiarities in cadherin function exist between developing and mature brain, the distribution of cadherins at a synapse varies with synapse age (Elste and Benson, 2006). Subsequent to generating adhesion at adherens junctions between neighboring cells, cadherins and actin are localized to the edges of the junction (Uchida et al. 1996;Adams et al., 1998), a localization that correlates with the observed clustering of α-N-catenin, a ubiquitous cadherin-

binding protein, at the edges of active zones in adult mice (Uchida et al., 1996). *In vivo* immunofluorescence/EM experiments in the middle molecular layer of mature dentate gyrus have demonstrated that N-cadherin remains clustered at synapses following LTP induction (Huntley et al., 2012), while the presence of cadherin-8 is diminished. These results suggest that cadherin localization is regulated by synaptic activity, and that the continued presence of N-cadherin during synapse enlargement may contribute to stabilization at regions of synaptic remodeling.

Another family of CAMs includes the heterotypic neurexins. Neurexin-1β has 2 postsynaptic partners: Neuroligin-1 (NLG-1) and Leucine-rich repeat transmembrane protein-2 (LRRTM2) bind Neurexin-1β (Nrx-1β) at excitatory synapses (Ichtchenko et al., 1995;Song et al., 1999;de Wit et al., 2009), and are necessary for normal synapse initiation and validation (Sudhof, 2008). Nrxs bind the scaffolding protein CASK (Mukherjee et al., 2008), and are necessary for the coupling between calcium channels and presynaptic release machinery (Missler et al., 2003). Both NLG-1 and LRRTM2 interact with NMDA receptors through binding with PSD-95 (Irie et al., 1997;Linhoff et al., 2009;Kornau et al., 1995) and indirectly with AMPA receptors by binding with stargazin and other transmembrane AMPAR-associated proteins (TARPs) (Bats et al., 2007; Shi et al., 2009). Furthermore, NLG-1 overexpression potentiates NMDAR/AMPAR mediated EPSCs, which is reversed with AP5 and chronic blockade of CAM-kinase II. Knockout of NLG-1 reduced NMDAR-but not AMPAR-mediated transmission and creates deficits in long-term potentiation (Chubykin et al., 2007; Jung et al., 2010). Knockdown of LRRTM2 significantly reduces the amplitudes of AMPAR/NMDAR mediated EPSCs (de Wit et al., 2009). Overexpressing Nlgs in culture results in increased number and size of synapses (Levinson et al., 2005;Ko et al., 2009), and downregulating Nlgs results in the opposite effect (Chih et al., 2005).Clearly, both of these post-synaptic CAMs are capable of signaling to recruit glutamate receptors and other PSD proteins to forming

synapses. Presynaptic nrx-1β also recruits post-synaptic elements to nascent synapses. Cells expressing nrx-1β induce clustering of NLG-1 and LRRTM2 (Siddiqui et al., 2010;Graf et al., 2004), and NLG-1 and LRRTM2 in turn recruit presynaptic elements. NLG-1/ Nrx-1β interactions are sufficient to induce the formation of functional vesicle release sites, and overexpression of LRRTM2 in culture promotes synapsin and VGLUT clustering (Dean et al., 2003;Linhoff et al., 2009). Neurexins and neuroligins/LRRTMs are therefore capable of engaging in bidirectional signaling that allows both pre- and postsynaptic proteins to initiate and propagate synapse formation, and perhaps enlargement.

Another CAM family, the ephrin axon guidance family, affects synaptic localization of NMDARs; knockout of all three ephrin-B receptors dramatically decreases excitatory synapse number (in developing and mature synapses) in the hippocampus (Henkemeyer et al., 2003;Kayser et al., 2006). In addition, direct extracellular contact between presynaptic ephrin-B receptors and postsynaptic EphB receptors during synapse formation leads to EphB and NMDAR clustering during synapse formation (Kayser et al., 2006). Presynaptic EphrinB2 expression enhances surface retention of GluR2 receptors (Dalva et al., 2000). Expression of EphB2 triggers clustering of synaptic vesicles and enriches ephrinBs at synapses (Kayser et al., 2006). As with neurexins and neuroligins/LRRTM2, bidirectional signaling allows both pre- and postsynaptic proteins to initiate and propagate synapse formation, and potentially synapse enlargement.

Of the molecules mentioned above, NCAM, cadherins, integrins, nectins, and neuroligins all possess the capacity to anchor themselves to the actin cytoskeleton, and many of the others affect actin dynamics, and can therefore possibly modulate transport of intracellular resources. During synaptogenesis, F-actin accumulates at contact sites (Dai and Peng, 1996;Zhang and Benson, 2002). Actin depolymerization in young neurons results in an almost complete loss of synapses, but does not affect basic synapse ultrastructure in mature

tissue (Zhang and Benson, 2001). Also, whereas isolated synaptosomes from developing brain are sensitive to calcium depletion and trypsin (Khaing et al., 2006; Zhang and Benson, 2001), those from mature tissue are not (Cotman and Taylor, 1972; Pfenninger, 1971; Zhang and Benson, 2001), indicating that, to some extent, young and mature synapses stabilize trans-synaptic adhesion in different ways.

Development of a new synapse into a mature synapse is prolonged with respect to synaptogenesis, as indicated by the time-course of ultrastructural (Ahmari and Smith, 2002) and electrophysiological (Bolshakov and Siegelbaum, 1995;Chavis and Westbrook, 2001;Liu and Tsien, 1995;Mohrmann et al., 2003;Tovar and Westbrook, 1999) maturation, and is dependent on dendritic spine morphogenesis (Yuste and Bonhoeffer, 2004;Tada and Sheng, 2006). In general, synaptic maturation involves synapses growing larger via increase in the amount of pre- and postsynaptic structures, including SSVs, presynaptic active zone proteins, postsynaptic ionotropic glutamate receptors, directly associated scaffolding proteins, and many other proteins that have not been studied in the context of the synaptogenesis timeline that may only engage well into maturation. There are underlying differences between synapses at various stages of development, stability, and age, but the processes of synapse formation and synapse enlargement undeniably have much in common, and may share ultrastructural correlates that are indicative of various phases of synapse enlargement.

One such potential correlate is the postsynaptic vesicle-free transition zone (VFTZ, Figure 1.1, Spacek and Harris, 1998), which we propose to rename here as the vesicle-free postsynaptic zone (VFPZ), in recognition that it is found at the postsynaptic density,. VFTZs are postsynaptic thickenings that occur primarily at the edges of synapses, and have no vesicles oriented vertically to the presynaptic membrane in the presynaptic axonal bouton. The VFTZ is a postsynaptic structure that is contiguous with the synaptic active zone (SAZ). The

SAZ has both a postsynaptic component, the portion of the postsynaptic density (PSD) that apposes presynaptic vesicles, and a presynaptic component, which includes the presynaptic active zone machinery and associated synaptic vesicles. The VFTZ could be a region in which new proteins have been recruited to the postsynaptic membrane adjacent to an enlarging PSD before presynaptic vesicles are recruited to the apposing presynaptic portion of the synapse. If VFTZs are the means by which a PSD enlarges, then they likely contain proteins that help coordinate postsynaptic and presynaptic plasticity. Bidirectional signaling at the synapse is provided by cell adhesion molecules, one of which, N-cadherin, has been shown to be localized to the edges of mature synapses (Uchida et al., 1996), possibly in VFTZs.

A clear candidate for a presynaptic correlate of synapse growth is the aforementioned DCV, as it transports active zone proteins piccolo, bassoon, cadherins, and other proteins that appear during vesicle clustering in synaptogenesis prior to the recruitment of postsynaptic receptors (Cases-Langhoff et al., 1996;Garner et al., 2000;tom et al., 1998;Zhai et al., 2000; Zhai et al., 2001). DCVs may be inserted at the edges of presynaptic active zones to expand the presynaptic portion of a growing synapse, extruding cadherins and other CAMs into the cleft, which then bind their postsynaptic partners, and providing for additional docking sites for newly recruited synaptic vesicles.

This work builds on an existing model of synapse enlargement following LTP induction (Bourne and Harris, 2008; 2011a). I hypothesized that a mature hippocampal synapse is enlarged by 1) the assembly of VFTZs which enlarge the PSD, 2) the insertion of presynaptic DCVs which enlarge the presynaptic active zone, and 3) the recruitment of additional presynaptic vesicles to allow for increased neurotransmitter release. By looking at synaptic ultrastructure at various time points following LTP induction, I have begun to unravel the sequence in which these processes occur.

Figure 1.1 The vesicle-free transition zone (VFTZ) is a postsynaptic thickening that is contiguous with the synaptic active zone (SAZ). It has no presynaptic vesicles oriented perpendicular to the presynaptic vesicle membrane. Scale bar is 0.5 μm (Figure from Harris and Spacek, 1998).

Chapter 2

Developing a Strategy to Analyze Vesicle-Free Transition Zones in Perfusion-Fixed Control Hippocampus

Both VFTZs and DCVs have been previously identified and quantified to some degree, but never in the same study. In order to do so, observations must be made at synapses at which presynaptic vesicles can be clearly discerned in order to determine whether or not VFTZs are present. Axonal boutons must be imaged completely and clearly so that all DCVs they contain can be measured. Any approach that requires that these criteria be met will necessarily restrict analyses to a subset of the existing synapses, which may result in a significant reduction in the number of synapses available for analysis or the introduction of a sampling bias. In this chapter, I address the issues arising from combining pre- and post-synaptic ultrastructural measurements in this way, and develop a methodology in perfusion-fixed mature hippocampus that can be applied to hippocampal LTP slice experiments in order to determine what role VFTZs and DCVs play in LTP-induced synapse enlargement.

2.1 Experimental Methods in Hippocampal Perfusion Fixed Control

Rapid perfusion fixation is widely accepted as the gold standard for anatomical analyses, as the fixative spreads through living tissue e(Lavenex et al., 2009;Roberts et al., 1990;Miller, 1998). This method of fixation best preserves cell morphology, therefore perfusion-fixed mature brain that has not undergone electrical stimulation from a exogenous source provides the most ideal tissue in which to begin identifying and measuring synaptic structures. The electron micrographs (EMs) of the perfusion fixed control tissue used for this purpose were obtained during earlier studies in the middle of stratum radiatum in area

CA1 of the hippocampus (Harris and Stevens, 1989;Spacek and Harris, 1997;Harris et al., 1992), described below.

Tissue Processing

Serial sections were obtained from a young adult male Long-Evans rat. The animal was anethestized with pentobarbital, and intracardiac perfusion was performed with fixative containing paraformaldehyde, glutaraldehyde, and $CaCl_2$ in cacodylate buffer with backing pressure from compressed gas. After one hour, the brain was disected, and 400 µm slices were taken from CA1. Slices were washed before undergoing dehydration through graded ethanols with uranyl acetate staining, followed by propylene oxide, and finally embedding in epoxy resin. The hardened epon blocks were hand trimmed before precision trimming to a trapezoid containing CA1 pyramidal cell bodies and the apical dendritic arbor on a Reichert Ultracut III ultramicrotome (Lerca, Deerfield, Illinois). One hundred and three serial sections of roughly 55 nm thickness were obtained and stained with lead citrate and then photographed with a JEOL 100B electron microscope (Peabody, MA). A calibration grid (Pella, Redding, CA) was photographed with each series in order to allow for quantitative measurements of the images and three-dimensional reconstructions in the RECONSTRUCT™ software [available for free download at http://synapses.clm.utexas.edu] (Fiala and Harris, 2001;Fiala, 2005).

2.2 Quantitative Measurements and Three-Dimensional Reconstructions

After being photographed, the section images were aligned and axonal and dendritic structures (e.g. the outlines of plasma membranes and PSDs) were traced across serial sections in RECONSTRUCT™. I used this series to develop the new strategy to study VFTZs.

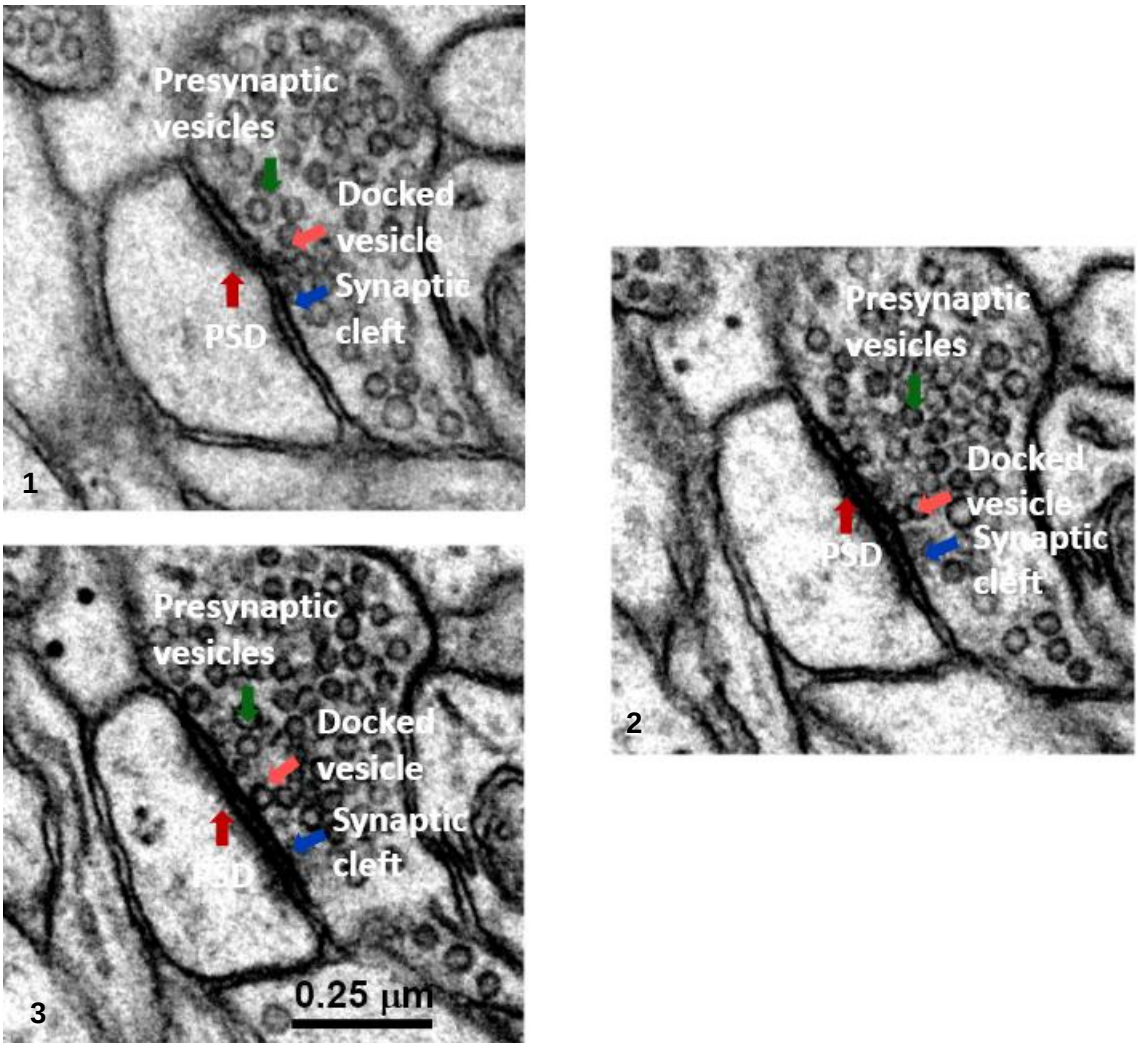

Figure 2.1 EMs of 3 serial sections through a synapse (ordered by number in the lower left hand corner of each image). The PSD (red arrow), presynaptic vesicles (green arrow), docked vesicles (pink arrow), and synaptic cleft (blue arrow) are all clearly visible on each section on which the synapse appears. Scale bar 0.25 μm

Figure 2.1 shows 3 EMs of serial sections through a synapse from those images. This particular synapse is cut entirely in cross-section, so the PSD, the presynaptic, the docked vesicles, and the synaptic cleft are visible on each section on which the synapse appears. For cross-sectioned objects, e.g. the PSD in Fig 2.1, area was quantified by placing open traces along the plasma membrane at the PSD (Fig 2.2, red line) on each section on which the synapse appears. Traces having the same name were connected across sections, and trace length was multiplied by section thickness and summed across sections to compute the PSD area. Closed traces (Fig, 2.2, dendritic spine in yellow) were used to generate 3D visualizations. Figure 2.3A shows 4 serial sections through a cross-sectioned synapse. The closed traces of the spine head (yellow), PSD (red), presynaptic vesicles (green), and VFTZ (blue) were used to generate the 3D representation in Fig. 2.3B. PSDs are not always so clearly sectioned as in this example. Figure 2.4 shows 3 EMs of serial sections through an obliquely cut synapse from the same tissue, in which one can make out the obliquely sectioned PSD and some presynaptic vesicles, but not the docked vesicles or synaptic cleft. To measure the area of oblique PSDs, a closed trace was placed around the perimeter of the PSD on each section on which the PSD appears (Fig 2.5). A connector was drawn to estimate where the areas overlapped on consecutive sections, and the closed traces were then trimmed to ensure that the overlapping area was only traced on one section. The total area equaled the enclosed areas plus the length of each connector multiplied by section thickness.

One sees these varying orientations of synapse sectioning within a series due to dendrite morphology. This variation poses a problem with respect to VFTZ analyses in that section thickness is ~55 nm and most presynaptic vesicles are less than 55 nm in diameter. Obliquely sectioned PSDs may therefore obscure some vesicles in the presynaptic terminal in EMs, and thus one cannot accurately determine whether a VFTZ is present at those synapses. Any VFTZ

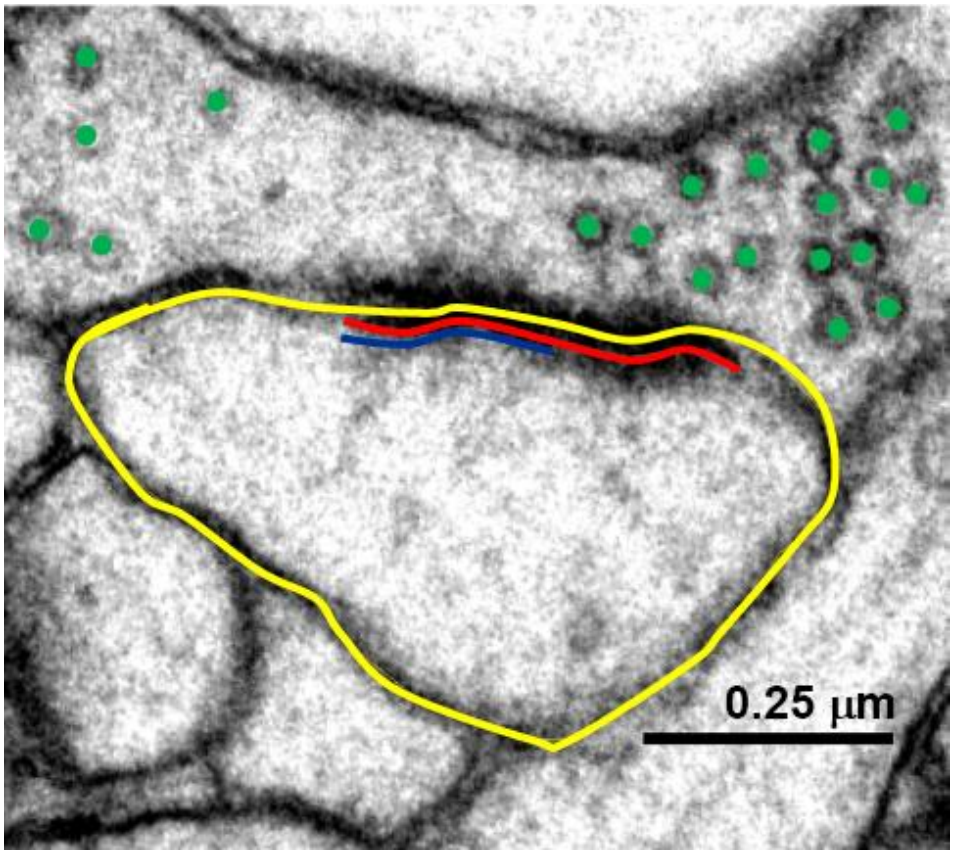

Figure 2.2 EM of a synapse with traces generated in RECONSTRUCT™ superimposed. Open red trace is used to compute PSD area. Open blue trace is used to compute VFTZ area. Closed yellow trace is used to generate 3D reconstruction of dendritic spine head. Green stamps are used to generate 3D reconstructions of presynaptic vesicles. Scale bar 0.25 μm

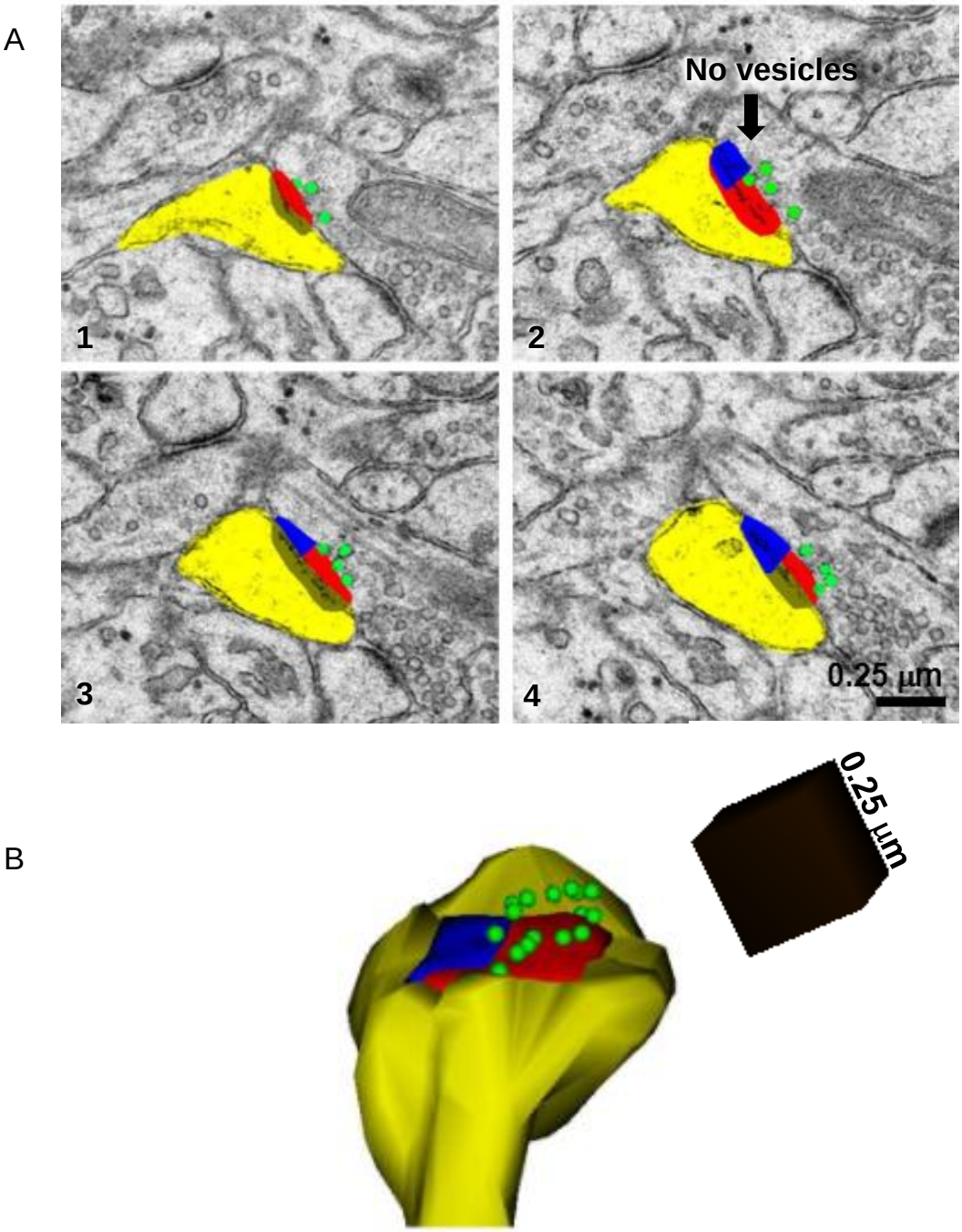

Figure 2.3 3D Reconstructions. A) EMs of 4 serial sections through a spine head with superimposed closed traces (ordered by number in the lower left hand corner). Spine head (yellow), PSD (red), VFTZ (blue) and presynaptic vesicles (green) traces were used to generate B) 3D reconstructions. Scale bar 0.25 μm. Scale cube 0.25 μm per side.

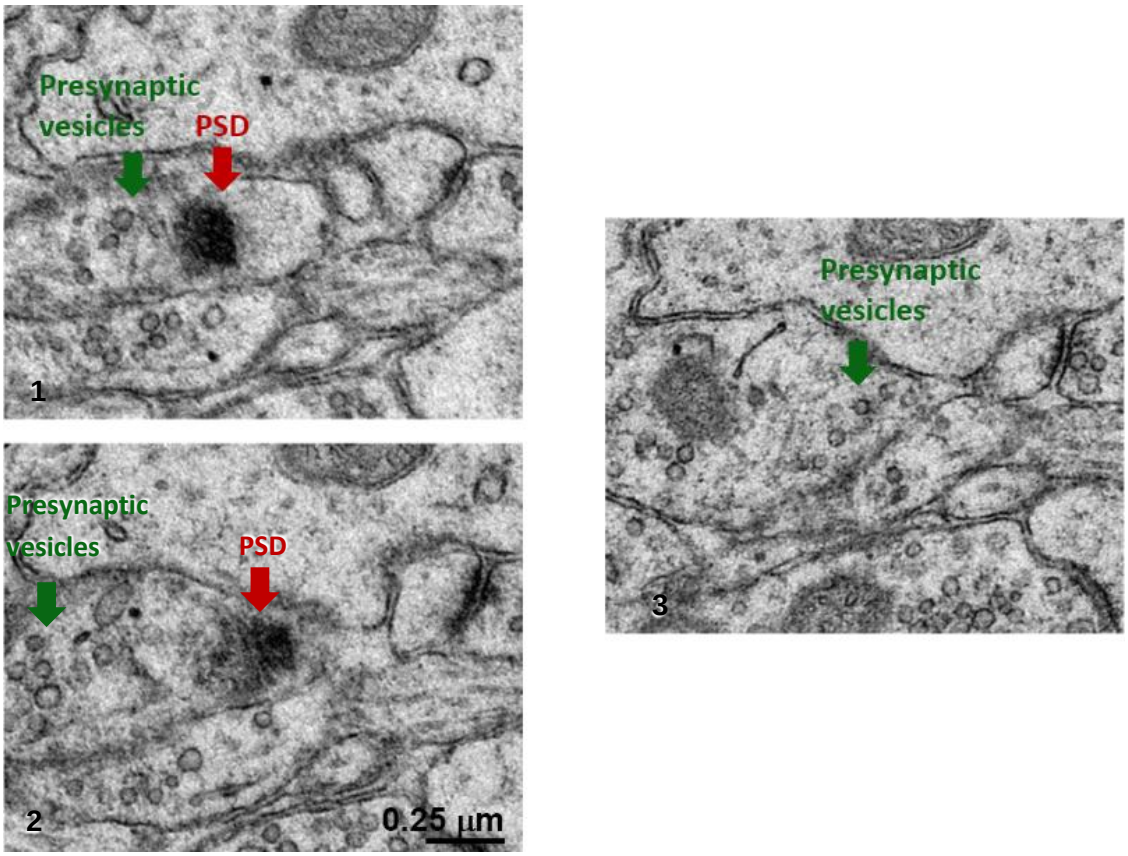

Figure 2.4 EMs of 3 serial sections through an obliquely sectioned synapse (ordered by number in the lower left hand corner of each image). The PSD (red arrow) and some of the presynaptic vesicles (green arrow) are visible on each section on which the synapse appears, but the docked vesicles and synaptic cleft are not. Scale bar 0.25 μm.

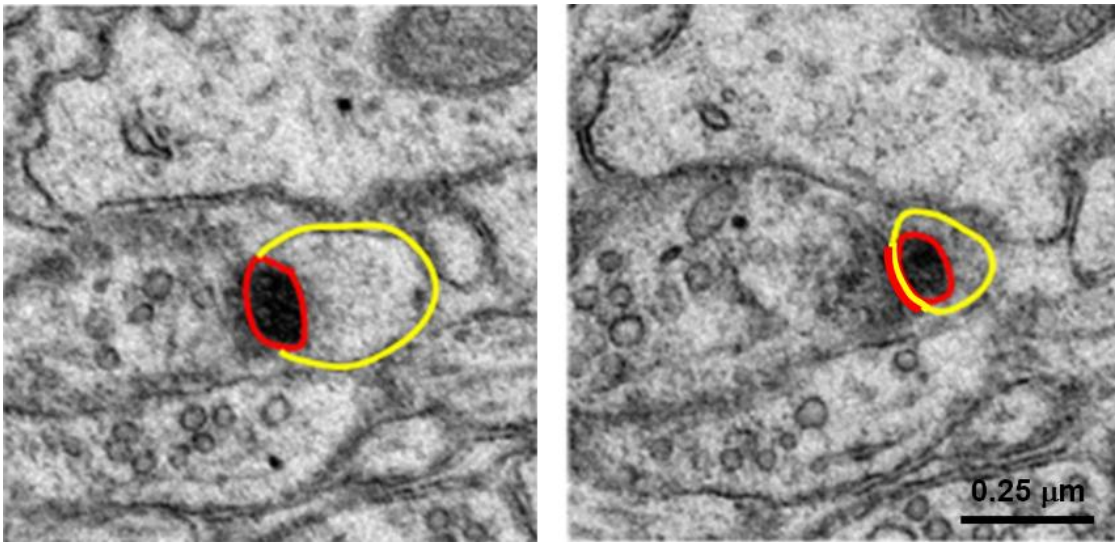

Figure 2.5 EMs of 2 serial sections through an obliquely sectioned synapse with traces superimposed. Red traces are used to compute the PSD area. Closed yellow trace is used to generate the 3D reconstruction of the dendritic spine. Scale bar 0.25 μm.

analyses must be restricted to cross-sectioned synapses, and it is therefore necessary to determine whether restriction to that subset of synapses introduces a bias. All PSDs on complete spines within a 216 μm^3 volume from this series were traced and divided into 4 categories based on sectioning orientation. Synapses were defined as “cross-sectioned” if they were in cross-section on each section on which they appeared. Synapses were defined as “oblique” if they were obliquely sectioned on each section on which they appeared. This was with the exception of slightly obliquely sectioned PSDs, which were treated as cross-sectioned if the presynaptic vesicles and plasma membranes were clearly visible, so that PSD size was not overestimated by including a portion of the depth of the PSD in the surface area measurement. Synapses were defined as “cross-sectioned/oblique” if they appeared in cross-section on some sections and were obliquely sectioned on others. The areas for cross-sectioned and obliquely sectioned portions of these synapses were measured independently as described above and then summed to obtain the entire area of the PSD. Synapses were defined as being “en-face” if the PSD was sectioned parallel to the synaptic cleft and therefore appeared on only 1 section (occasionally 2, depending on PSD volume). Cross- sectioned PSD areas span the entire range of PSD areas (Fig 2.6), therefore VFTZ analyses can be restricted to cross-sectioned synapses without excluding a particular subset based on area. The PSD area was measured on all cross-sectioned synapses on complete spines (spine is not cut off by the edges of a section or the beginning or end of the series) along 7 dendritic segments of similar length and caliber. This matched-caliber dendritic analysis ensures that spine density does not vary greatly between different dendritic segments and impact any other measurements.

Before beginning the VFTZ measurements, it was necessary to define what constitutes a VFTZ. The smallest VFTZ could be one vesicle diameter wide, as that is the size of a docking site. But a region that small could also be a location at which a vesicle has just been released and to which another one has

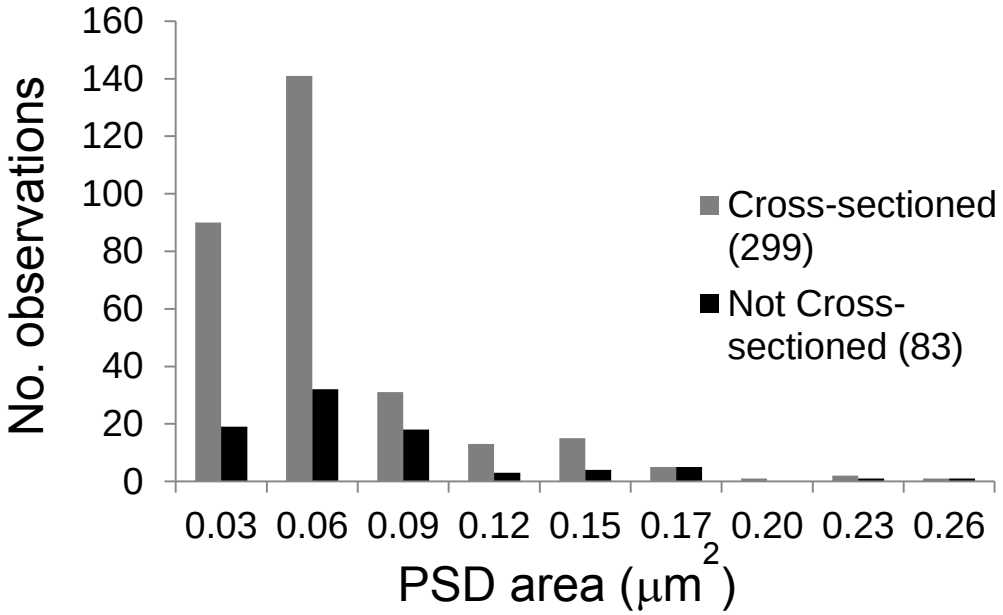

Figure 2.6 Distribution of surface areas of cross-sectioned PSDs (gray) and the area of PSDs that are not cross-sectioned (black). PSD areas of cross-sectioned synapses span the entire range of PSD areas (n = number of synapse).

not yet docked. The definition of the VFTZ is therefore more conservative; a VFTZ is at least 2 vesicle diameters wide and has no apposing presynaptic vesicles (SSVs) within 2 vesicle diameters orthogonal to the presynaptic membrane. In order to determine the mean SSV diameter, it is practical to restrict the diameter measurement to a subset of all SSVs in the series. As was done in a previous study (Sorra et al., 2006), I first identified DCVs in axonal boutons synapsing on the spine synapses on the dendrites chosen above. Figure 2.7 shows an example of a presynaptic DCV (red arrow) from this series; it has a dense core that is distinct from its membrane. A circular trace was placed on the outer DCV membrane at its widest point. The circumference (C) of this trace was used to compute diameter (D) for each DCV ($D = C/\pi$). The SSV closest to each DCV (Fig 2.7, green arrow) was identified, and it circumference and diameter were measured and computed in the same way as for DCVs. The minimum VFTZ length was then defined as twice the mean of the diameters of the SSVs identified as being closest to each DCV traced. The mean SSV diameter was 0.047 μm, so the minimum VFTZ length was defined as being 0.094 μm. Once the minimum VFTZ length was determined, VFTZs were identified and measured on all cross-sectioned spine synapses on the dendrites chosen above. SSVs close to the presynaptic membrane were stamped (Fig 2.2, green circles). Linear traces were drawn from those SSVs to the presynaptic membrane in order to determine that the distance between them was at least 2 mean SSV diameters (0.094 μm). PSD traces were copied, pasted, and truncated to the appropriate region based on these distances and renamed as VFTZs (Fig. 2.2, blue line). VFTZ areas and reconstructions were computed in the same manner as PSD areas, as follows. VFTZ area was quantified by placing open traces along the plasma membrane at the PSD (Fig 2.2, blue line) on each section on which the VFTZ appears. Traces with same name were connected across adjacent sections, and trace length was multiplied by section thickness and summed across sections to compute the VFTZ area. Closed traces (Fig, 2.2, dendritic

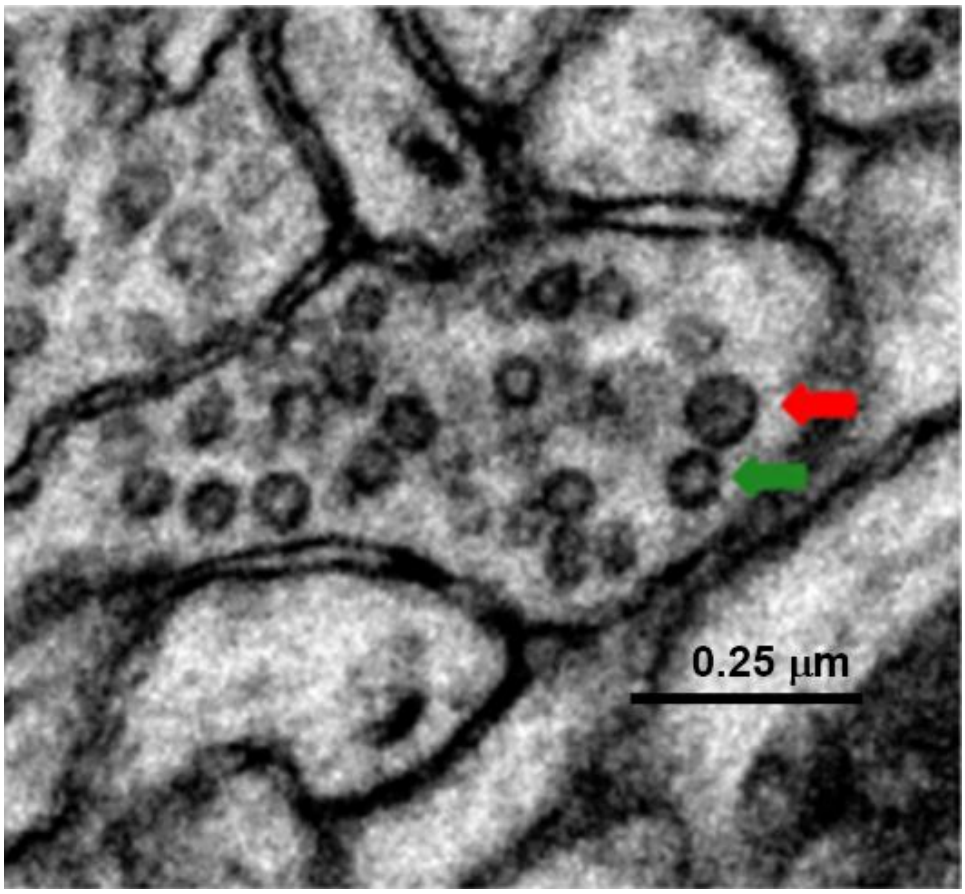

Figure 2.7 EM of DCV (red arrow) and its closest SSV (green arrow). The mean diameter of those SSVs that are the closest to each DCV identified in boutons synapsing on the cross-sectioned spine synapses on dendrites included in the postsynaptic analyses. Scale bar 0.25 μm.

spine in yellow) were used to generate 3D visualizations. Areas of VFTZ that were not continuous either within a section or across consecutive sections were treated as separate individual VFTZs. The total number of synapses analyzed in this manner was 134. For the analyzed synapses, the proportion of PSDs that had VFTZs was 0.34, and the average number of VFTZs per PSD was 0.36 +/- 0.05. Figure 2.8A shows the distribution of the areas of the individual VFTZs, which range from 0.0048 μm^2 to 0.0509 μm^2, with a mean of 0.0114 +/- 0.0012 μm^2 (n = 49). Figure 2.8B shows the distribution of the areas of total VFTZ areas for each PSD that has VFTZ(s). Areas range from 0.0048 μm^2 to 0.0591 μm^2, with a mean of 0.0122 +/- 0.0014 μm^2.

For the DCV analysis, the total number of synapses analyzed was 120, as the analysis was restricted to complete boutons synapsing on spines from the VFTZ analysis. For those synapses, the proportion of PSDs synapsing with boutons that have DCVs was 0.34, and the average number of DCVs per bouton was 0.76 +/- 0.12. Figure 2.9 shows the diameter distributions of DCVs and their closest neighboring SSVs in boutons synapsing on spines included in the VFTZ analysis. DCV diameters range from 0.051 μm^2 to 0.103 μm, with a mean of 0.074 +/- 0.001 μm (n = number of DCVs/SSVs, 80), and SSV diameters range from 0.034 μm to 0.066 μm, with a mean of 0.047 +/- 0.001 μm. (n = number of DCVs/SSVs, 80). These numbers are comparable to those from previous studies (Sorra et al., 2006). The ratio of sum of the VFTZ area for all synapses to the sum of the PSD area for all synapses was ~0.08. These results together indicate that VFTZs are both countable and measurable

To summarize, I have established a methodology that allows for the restriction of the VFTZ analysis to cross-sectioned spine synapses in a matched dendrite analysis combined with an analysis of DCVs in boutons synapsing with those spines. This methodology defined the minimum VFTZ length as twice the mean vesicle diameter, which was calculated by averaging the diameters of the SSV nearest neighbor for each DCV identified in boutons synapsing at these

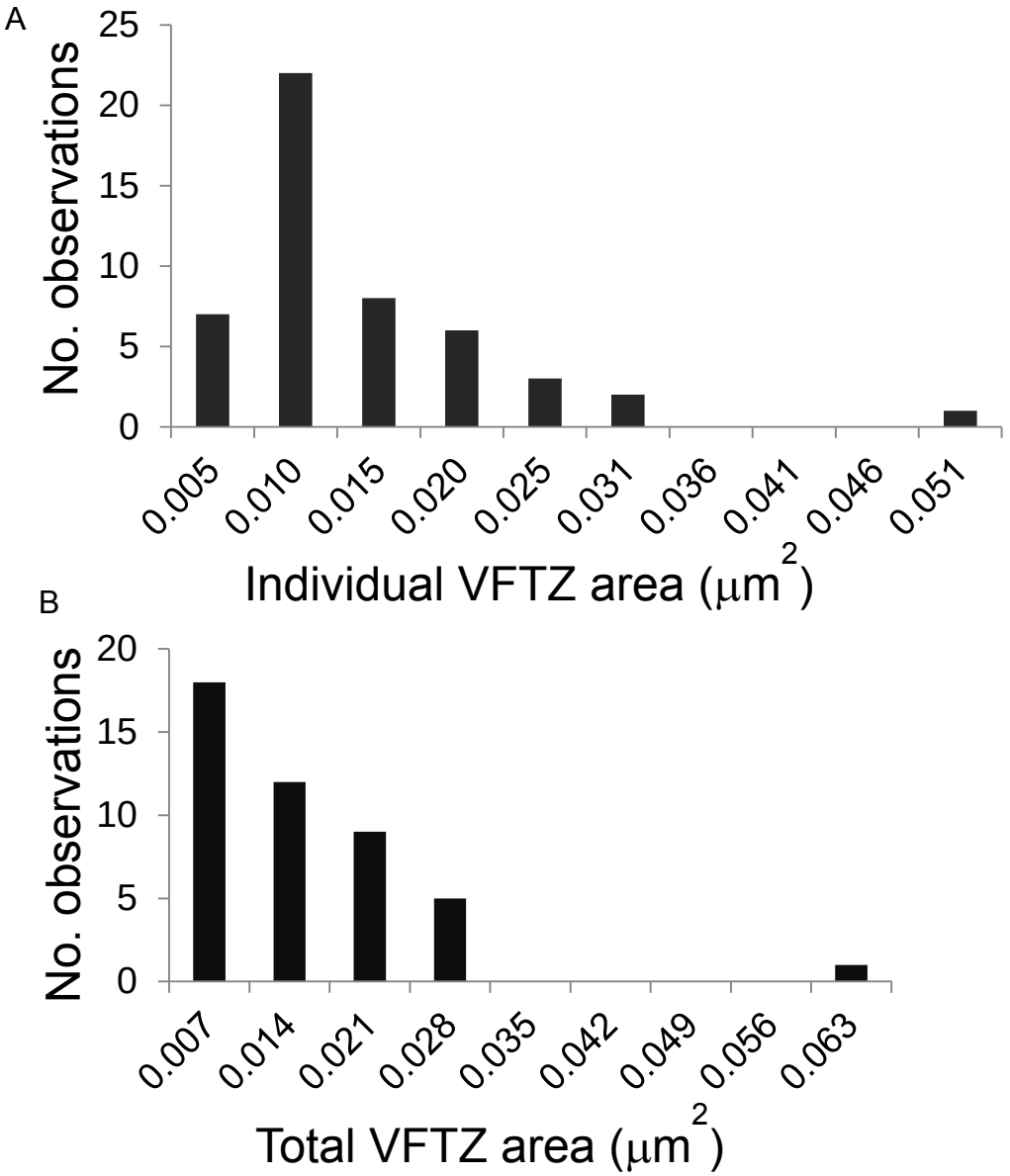

Figure 2.8 VFTZ areas. A) Individual VFTZ areas. Areas range from 0.0048 μm^2 to 0.0509 μm^2, with a mean of 0.0114 +/- 0.0012 μm^2 (n = number of VFTZs, 49). B) Total VFTZ areas. Areas range from 0.0048 μm^2 to 0.0591 μm^2, with a mean of 0.0122 +/- 0.0014 μm^2. (n = number of PSDs with VFTZs, 46).

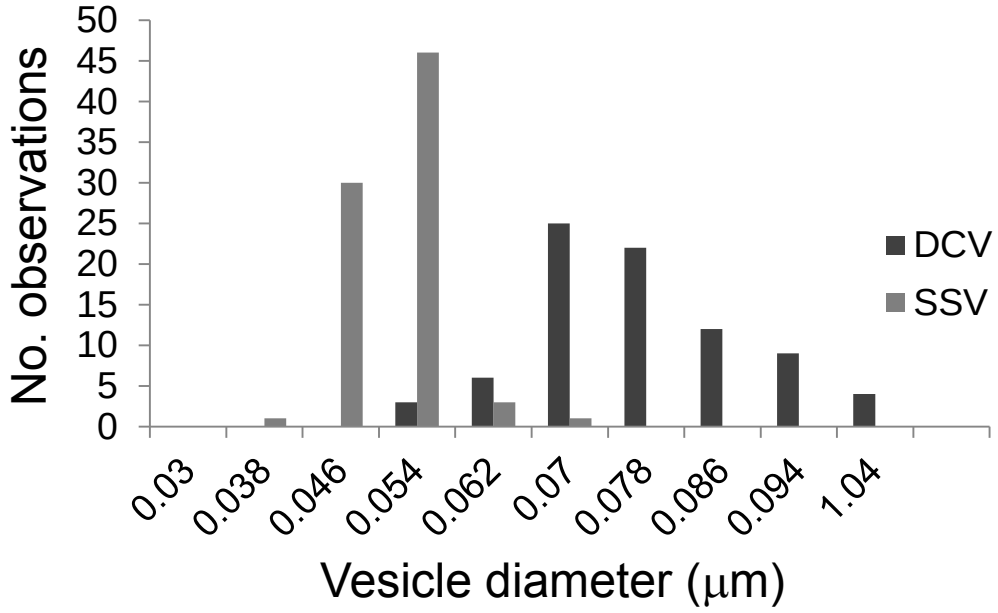

Figure 2.9 Vesicle diameters. DCV diameters range from 0.051 μm^2 to 0.103 μm, with a mean of 0.074 +/- 0.001 μm (n = number of DCVs/SSVs, 80). SSV diameters range from 0.034 μm to 0.066 μm, with a mean of 0.047 +/- 0.001 μm. (n = number of DCVs/SSVs, 80).

cross-sectioned synapses. The mean diameters of both vesicle types identified in this way were comparable to those calculated in other studies, and the frequency of DCVs and the frequency and size of VFTZs in perfusion fixed mature CA1 were significant and quantifiable. This methodology was then applied to EMs from previously conducted rat hippocampal CA1 acute slice experiments (Bourne and Harris, 2011a) and is explored in the next two chapters.

Chapter 3

Postsynaptic Enlargement Occurs via Vesicle-Free Transition Zone Growth by 2 Hours Following LTP Induction

Once the methodology was established for identifying and tracing DCVs, SSVs, and VFTZs at perfusion fixed control synapses, those measurements were performed in series from previously conducted LTP slice experiments (Bourne and Harris, 2011a) in order to determine the role that VFTZs play in synapse enlargement.

3.1 Methods and Previous Findings in LTP Hippocampal Slice Experiments

Preparation of and Recording from Hippocampal Slices

400 μm thick hippocampal slices were cut from eight young adult male Long Evans rats. The animals were anesthetized, decapitated, and slices were rapidly chopped. Slices were immediately placed in ACSF then recovered in an interface chamber at 32^{o}C for roughly 3 hours. Two concentric bipolar stimulating electrodes (100 μm outside diameter, Fred Haer, Brunswick, ME) were placed 300–400 μm on either side of a single extracellular recording electrode, which was located in the middle of stratum radiatum (Fig. 3.1A, arrow), for a separation of 600–800 μm between recording electrodes, which ensured that independent populations of inputs to CA1 pyramidal neurons were stimulated (Sorra and Harris, 1998;Ostroff et al., 2002). Extracellular field potentials were recorded and the slope (mV per ms) of the field excitatory postsynaptic potential (fEPSP) was measured.

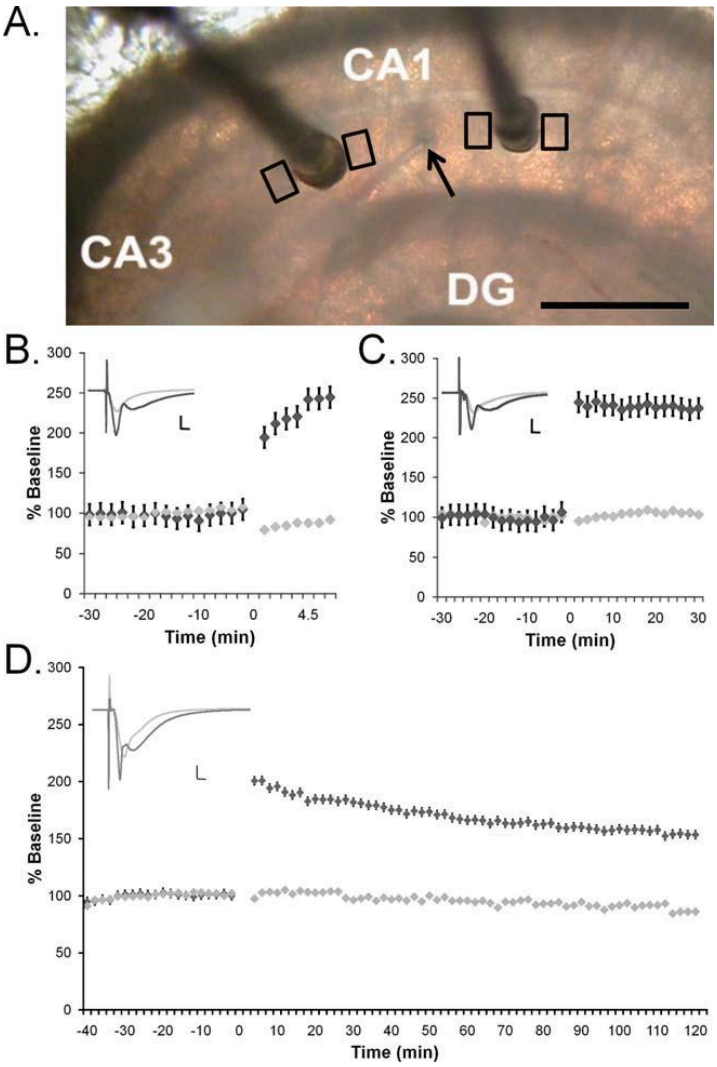

Figure 3.1 Site-specific TBS-LTP in hippocampal slices from adult rats. (A) A single recording electrode (arrow) was positioned in the middle of s. radiatum midway between two stimulating electrodes (dark posts). Tissue for analyses was collected immediately adjacent to the stimulating electrodes (black boxes) after microwave-enhanced fixation. Scale bar 5 500 lm. Theta burst stimulation(TBS) was delivered to one of the stimulating electrodes at time 0 to induce LTP (dark gray diamonds) while baseline stimulation was maintained at the other electrode (light gray diamonds). The responses were monitored for (B) 5 min (n = 3 slices from three animals), (C) 30 min (n = 3 slices from three animals), or (D) 2 h (n = 2 slices from two animals) after the delivery of the first theta burst stimulation. Example waveforms for each time (insets) are an average of the pre-TBS and post-TBS responses at the control (light gray) and TBS-LTP (dark gray) sites. Scale bars = 5 mV/5 μs. (Figure from Bourne and Harris, 2011a).

TBS-LTP Paradigm

One slice was used per animal. A stable baseline was established for 30 min and then theta burst stimulation (TBS) (8 trains of 10 bursts at 5 Hz of 4 pulses at 100 Hz delivered 30 s apart) was delivered to the stimulating electrode, and the control electrode received test pulses. The positions of the control and TBS-LTP electrodes were alternated between the CA3 and subicular side of the recording electrode across experiments. Responses from the control and TBS stimulating electrodes were recorded for up to 5 min, 30 min, or 2 h after the delivery of the first train of TBS (Fig. 3.1B–D). Only the slices demonstrating high-quality physiology were fixed and processed for electron microscopy (Bourne and Harris, 2011a).

Fixation and Processing for ssTEM

Hippocampal slices were immediately fixed after recording was completed in a microwave enhanced procedure (Jensen and Harris, 1989) and processed for ssTEM (Harris et al., 2006). The slices were fixed by immersion in glutaraldehyde and paraformaldehyde in a cacodylate buffer during a short burst of microwave irradiation and were maintained at room temperature in the same fixative overnight (Jensen and Harris, 1989). The slices were rinsed, embedded in agarose, and trimmed to a trapezoidal region of CA1 that contained both of the stimulating electrodes. Slices were then vibra-sliced (Leica VT 1000S, Leica, Nussloch, Germany), and the vibra-slice which showed a visible surface indentation slice plus the two located on either side of it were collected for each experiment (see black boxes in Fig. 3.1A). Vibra-slices were stained with osmium and potassium ferrocyanide in a cacodylate buffer, rinsed with buffer, immersed in osmium and microwaved, and rinsed again. Vibra-slices were dehydrated with graded ethanols containing uranyl acetate and microwaved after each transfer. Finally, slices were transferred through propylene oxide at room temperature, embedded in LX112, and cured for 48 hours in an oven (Harris et al., 2006). Test

thin sections that spanned the depth of the slice from air to net surface were taken and evaluated from each experiment. Only slices with a band of high quality tissue in both the control and TBS-LTP sides were included in the analyses. Of the 24 experiments, 16 were excluded because they did not meet anatomical criteria.

Three Dimensional Reconstructions and Measurements

Serial sections were cut from a trapezoid containing indentations from either the control or TBS-LTP stimulating electrode (see black boxes in Fig. 3.1A) and were mounted on Pioloform-coated slot grids (Synaptek, Ted Pella). Sections were counterstained with saturated ethanolic uranyl acetate and then with Reynolds lead citrate for 5 min each. Sections were imaged, blind as to condition, on a JEOL 1230 electron microscope with a Gatan digital camera at 5,000 x magnification. The serial section images were aligned, and PSDs were traced in RECONSTRUCT^{TM} . PSD areas were measured taking into account the orientation in which they were sectioned as described in Chapter 2.

Statistical Analyses

Statistical analyses were done in the STATISTICA software package (StatSoft, Tulsa, OK). Either a two-way ANOVA (condition and experiment) or a nested hierarchical ANOVA (dendrite nested in condition and experiment) was used to determine whether TBS-LTP had a significant effect on spines or PSDs. The number of synapses analyzed is indicated in each figure. All data are expressed as mean and S.E.M. or as described in specific figure legends (Bourne and Harris, 2011a). Spines were divided into three categories based on size: small, medium, and large. The “large” spines were both few in number and much larger than those in the other two categories; the distribution of spine size showed large gap between the largest of the small/medium spines and the smallest of the large spines. Therefore looking at changes in spine and synapses

by dividing them by size into these categories allows us to uncover effects of LTP that would otherwise have been masked by a disproportion in Ns.

Sample Dendrites

Cross-sectioned radial oblique dendritic segments that spanned at least 100 sections and had diameters between 0.4 and 0.8 μm were selected for analysis in order to ensure that differences in dendrite caliber were not sufficient to impact spine density under control conditions. Spine densities were within the range of those measured along oblique CA1 dendrites in adult, perfusion-fixed hippocampus for all time points and experimental conditions.

Previous Findings

Initial studies of these series measured postsynaptic changes on dendritic spines (Bourne and Harris, 2011a). Spines were categorized as being small, medium, or large based on head diameter. Head diameter was measured by drawing a linear trace parallel to the PSD on the section on which the spine head was widest. Small spines were defined as having a head diameter of less than 0.45 μm, medium spines were defined as having a head diameter between 0.45 μm and 0.6 μm, and large spines were defined as having a head diameter of 0.6 μm or greater. Figure 3.2A-C show single EMs of PSDs in cross-section on each of these 3 spine types; 2.2A shows a small spine, 2.2B shows a medium spine, and 2.2C shows a large spine. Figure 3.2D-F show the 3D reconstructions generated in RECONSTRUCT™ of the spines shown in Fig 3.2A-C. The PSD area was measured on each of these spine types along dendritic segments of similar length and caliber in these series as described previously. PSD size increased on spines of all sizes by 2 hours after LTP induction, as illustrated in Fig 3.3. If the VFTZ is indeed the unit by which the postsynaptic portion of a synapse can expand, then the increase in PSD area should be achieved by the

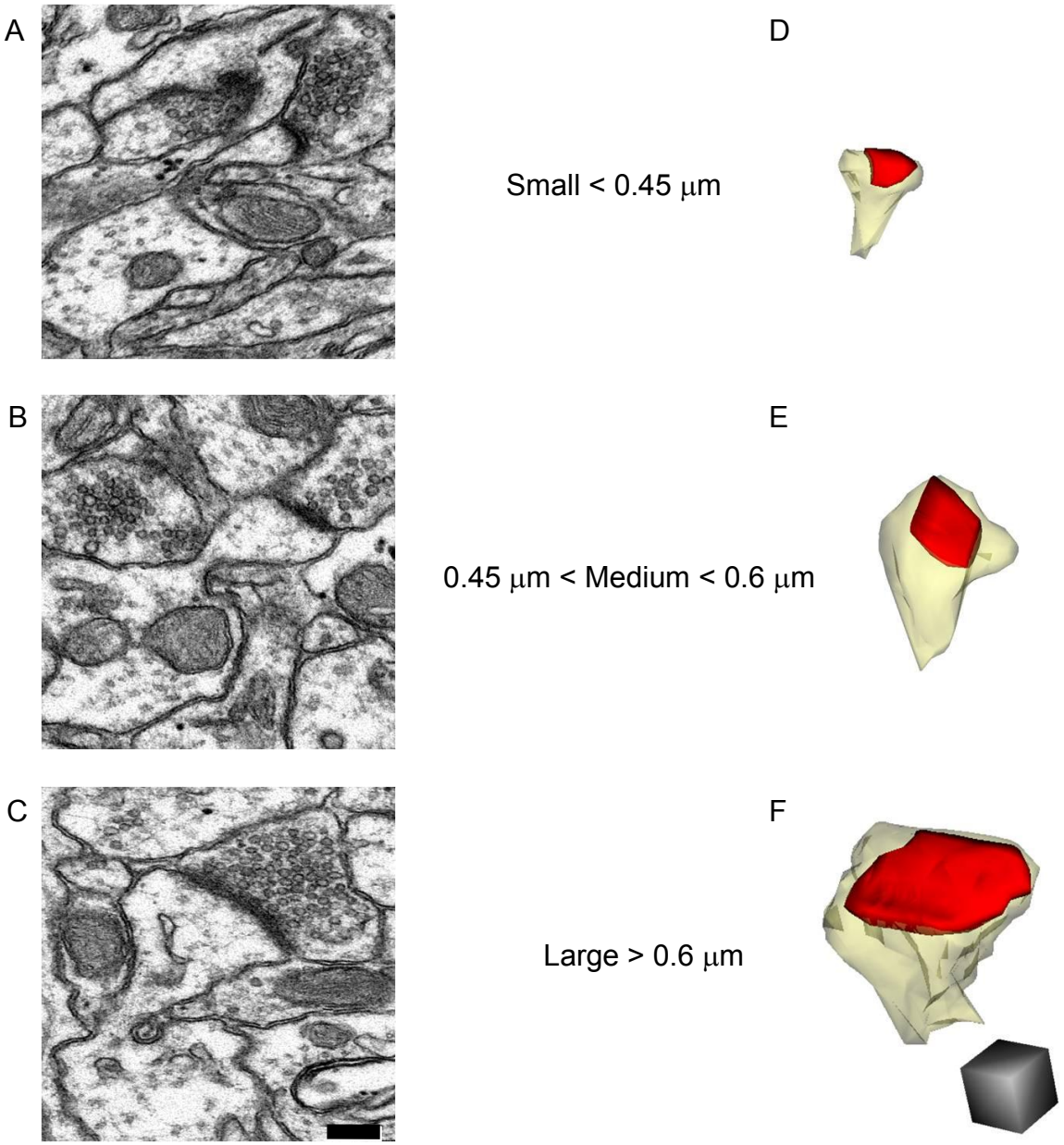

Figure 3.2 A-C Single EMs of asymmetric PSDs on A) a small spine head B) a medium spine head C) a large spine head from the CA1 slice tissue. D-F 3D reconstructions of the spines and PSDs shown in A-C. Spine heads are shown in yellow, PSDs are shown in red. Scale bar, 0.25 μm. Scale cube, 0.25 μm per side. (Figure modified from Bourne and Harris, 2011a)

-

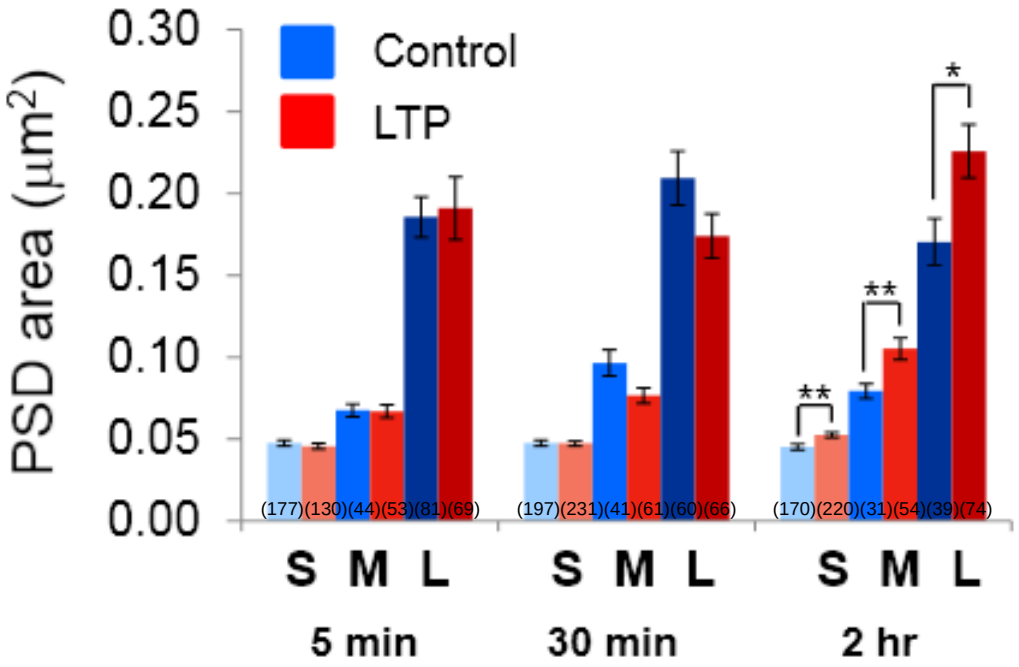

Figure 3.3 PSD enlargement by 2 hr following LTP induction. Blue shades indicate control dendrites (light blue: small spines, medium blue: medium spines, dark blue: large spines) and red shades indicate LTP dendrites (light red: small spines, medium red: medium spines, dark red: large spines). S = small spine, M = medium spine, L = large spine. At 2 hr PSD area was increased on spines of all sizes (n = number of synapses, * $P < 0.05$, ** $P < 0.01$, Figure adapted from Bourne and Harris, 2011a).

growth of or addition of VFTZs. I therefore hypothesized that the PSD enlargement corresponds to the growth of VFTZs at 2 hours after LTP induction.

3.2 VFTZ Frequency, Distribution, and Area

Using the approach developed in perfusion-fixed control hippocampus (Ch2), DCVs, SSVs, and VFTZs were measured on all cross-sectioned PSDs found in Bourne and Harris, 2011a. Spines were again divided into 3 categories based on spine head diameter. Figure 3.4 shows examples of VFTZs on each spine size. Figure 3.4A shows a small thin spine with a VFTZ, shown in blue, contiguous with part of the SAZ, shown in red, which apposes a docked vesicle (green arrow). Figure 3.4B shows a VFTZ (blue) adjacent to part of the SAZ (red) on a medium spine. Figure 3.4C shows 2 VFTZs adjacent to the SAZ on a large spine head synapsing on a bouton containing 2 DCVs (red arrows). Insets are the 3D reconstructions of the spines in 3.4A-C, where spine heads are in yellow, VFTZs are in blue, and SAZs are in red. Both the fraction of PSDs that have VFTZs (Fig 3.5A) and the number of separate VFTZs per PSD (Fig. 3.5B) were measured for spines of all sizes at 30 minutes and 2 hours following LTP induction. Control data is shown in shades of blue (light blue: small spine, medium blue: medium spine, dark blue: large spine.) LTP data is shown in shades of red (light red: small spine, medium red: medium spine, dark red: large spine). While the fraction of synapses that has VFTZs did not change with LTP induction for any spine type at either time point, more large spines had VFTZs than smaller spines (χ^2: $p < 0.05$). Similarly, while the number of VFTZs each synapse has did not change with LTP induction for any spine type at either time point, large spines had more individual VFTZs than smaller spines (χ^2: $p < 0.05$).. Both results indicate that larger spines are more likely to have VFTZs than their smaller counterparts, which is consistent with the finding that the PSDs that grew the most at 2 hours after LTP induction were those found on large spines (Fig

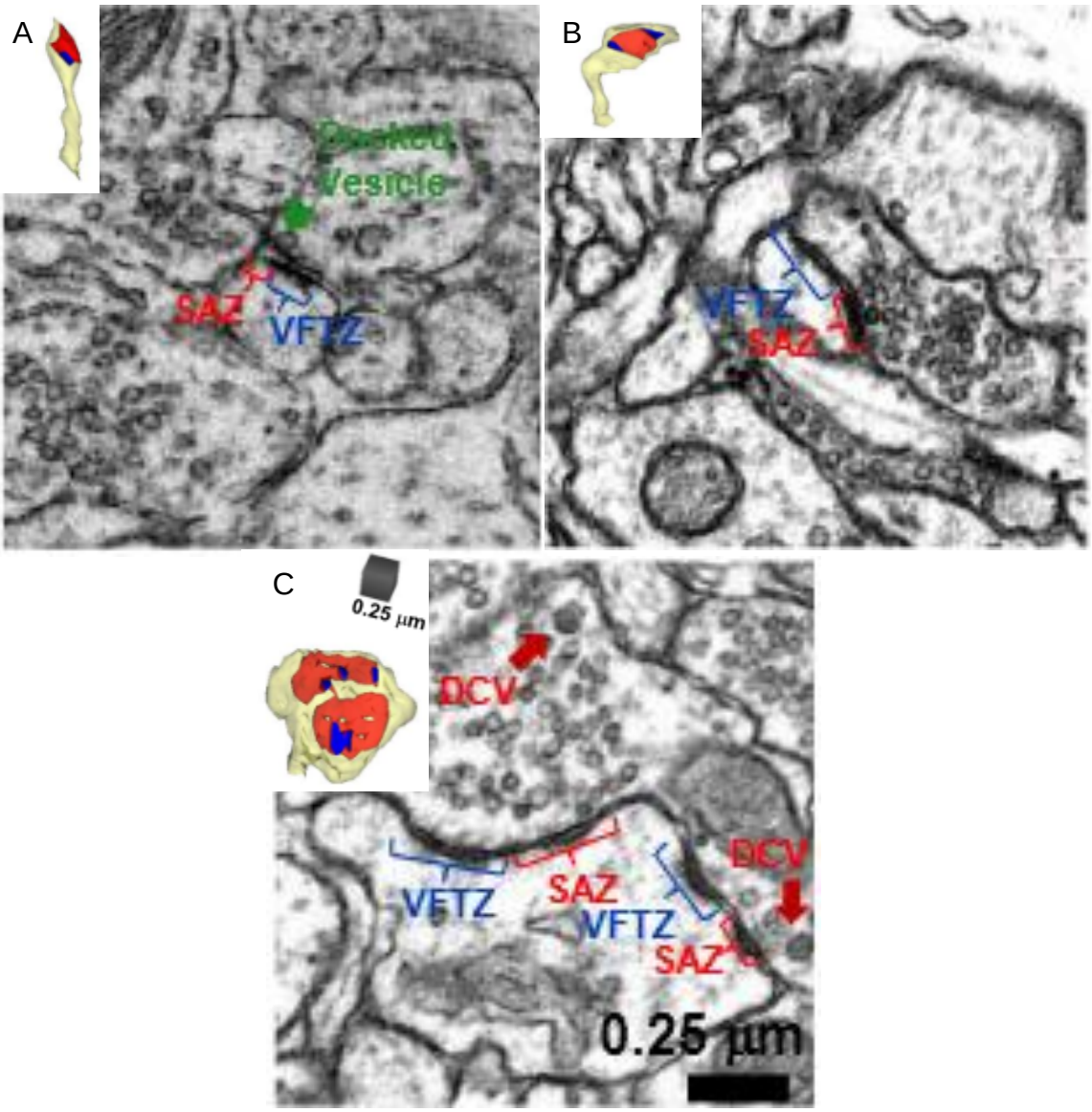

Figure 3.4 VFTZs on spines of all sizes. VFTZs are shown in blue, SAZs in red, spine heads are shown in yellow. A-C EMs of VFTZs on small, medium and large spines. Insets show 3D reconstructions of the spines in the EMs. A) VFTZ adjacent to SAZ apposing docked vesicle (green arrow) on small spine. B) VFTZ adjacent to SAZ on medium spine. C) Two VFTZs adjacent to SAZ on large spine head synapsing on a bouton containing two DCVs (red arrows). Scale bar, 0.25 μm, Scale cube 0.25 μm per side.

A

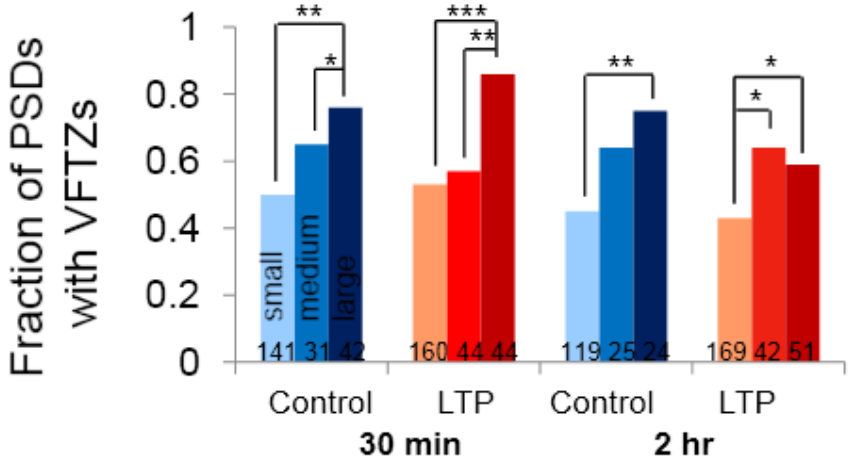

B

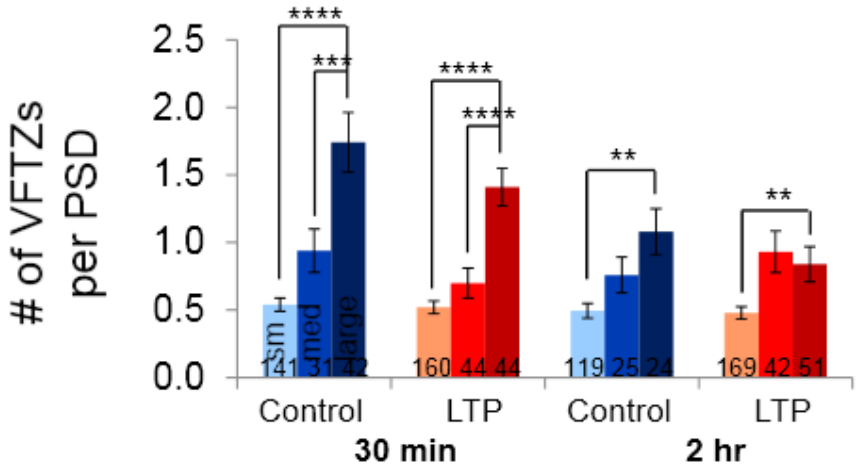

Figure 3.5 VFTZ frequency at 30 min and 2 hr following LTP induction on all spine sizes. Control data is shown in shades of blue (light blue: small spine, medium blue: medium spine, dark blue: large spine.) LTP data is shown in shades of red (light red: small spine, medium red: medium spine, dark red: large spine). A) Fraction of synapses that has VFTZs does not change with LTP induction for any spine type at either time point. More large spines have VFTZs than smaller spines. B) The number of individual VFTZs per PSD (includes zeroes) does not change with LTP induction for any spine type at either time point. Large spines have more individual VFTZs than smaller spines. (n = number of synapses, * $P < 0.05$, ** $P < 0.001$, *** $P < 0.0001$, **** $P < 0.00001$).

3.3). If the VFTZ is indeed the means by which synapses enlarge, one would expect to find them more frequently on spines that are growing the most.

VFTZ area was also measured at 30 minutes and 2 hours following LTP induction on all spine sizes. Figure 3.6 shows this data for synapses that have VFTZs. LTP data is shown in shades of red (light red: small spine, medium red: medium spine, dark red: large spine). Figure 3.6A shows that individual VFTZ area, the area of a region of a single VFTZ, decreased on small spines at 30 minutes and increased on small and large spines at 2 hours after LTP induction. Figure 3.6B shows that total VFTZ area per PSD, the sum of the individual VFTZ areas for each PSD, decreased on small and large spines at 30 minutes and furthermore, increased on spines of all sizes at 2 hours after LTP induction. Because there was no PSD growth at 30 minutes, this indicates that additional presynaptic vesicles were recruited to synapses on small and large spines by 30 minutes, and that VFTZ growth, at least in part, accounts for PSD growth that occurs by 2 hours after LTP induction.

In order to determine if VFTZ growth accounts entirely for PSD enlargement at 2 hours after LTP induction, it was necessary to look at postsynaptic active zone area (post-SAZ, Fig. 1.1), which is defined as the portion of the PSD apposed to presynaptic vesicles. Post-SAZ area was calculated by subtracting total VFTZ area (Fig 3.6B) from total PSD area at each synapse on spines of all sizes at 30 minutes and 2 hours following LTP induction. Post-SAZ area was unchanged at 30 minutes on all spine types, which is consistent with the lack of PSD growth at this time. At 2 hours, while both VFTZ and post-SAZ growth contributed to PSD enlargement on small and medium

A

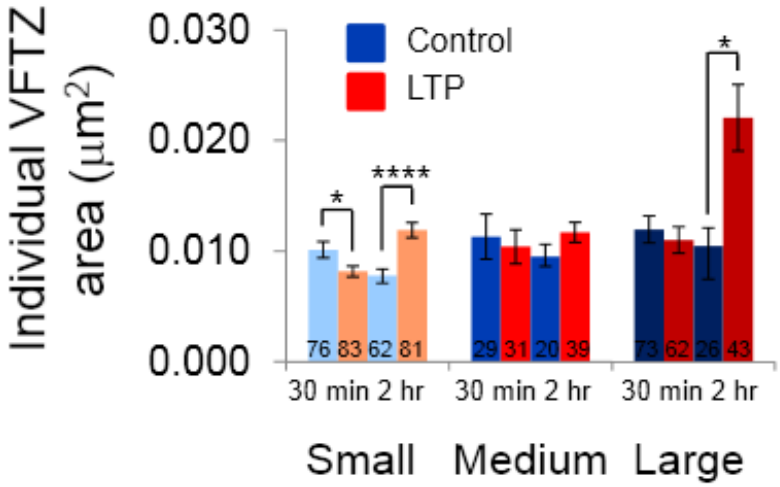

B

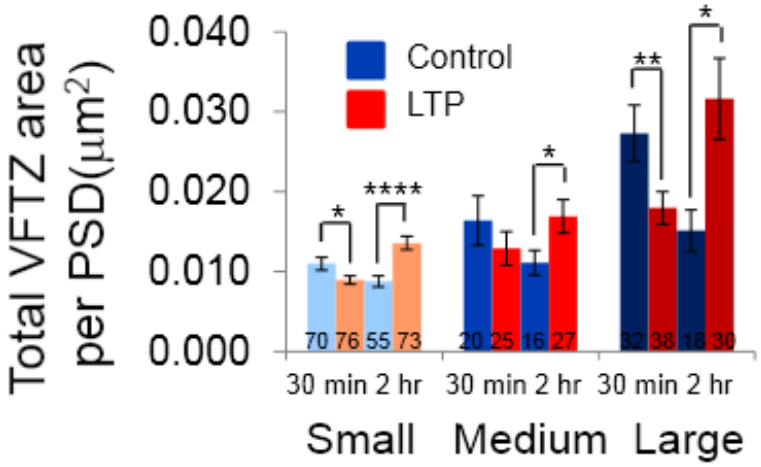

Figure 3.6 VFTZ area at 30 min and 2 hr following LTP induction on all spine sizes. Control data is shown in shades of blue (light blue: small spine, medium blue: medium spine, dark blue: large spine.) LTP data is shown in shades of red (light red: small spine, medium red: medium spine, dark red: large spine). A) Individual VFTZ area decreases on small spines at 30 min, and increases on small and large spines at 2 hr after LTP induction (n = number of individual VFTZs). B) Total VFTZ area per PSD decreases on small and large spines at 30 min, and increases on spines of all sizes at 2 hr after LTP induction (n = number of summed VFTZs). * $P < 0.05$, ** $P < 0.001$, **** $P < 0.00001$.

spines, post-SAZ area did not increase on large spines, therefore VFTZ growth accounts entirely for the enlargement of the largest PSDs. One possible reason for the lack of post-SAZ growth on large spines at 2 hours after LTP induction could be that because those are the PSDs that grew the most, the presynaptic region is still assembling the new presynaptic active zone machinery apposing the enlarged VFTZs, a process which may take longer than at the smaller spines, since their PSDs did not grow as much. It would be interesting to look at a later time point following LTP induction to determine whether additional vesicles are recruited to those VFTZs to enlarge the large spine SAZs at a delay with respect to those on smaller spines. It is also possible that enhanced release and replenishment of the docked vesicle pool depleted the non-docked vesicles closest to the presynaptic active zone to a greater degree in the large spines, thereby increasing the VFTZ area to a greater degree at 2 hours on those spines. The analysis of presynaptic vesicles in Chapter 3 will help to determine whether this explanation could be a valid one.

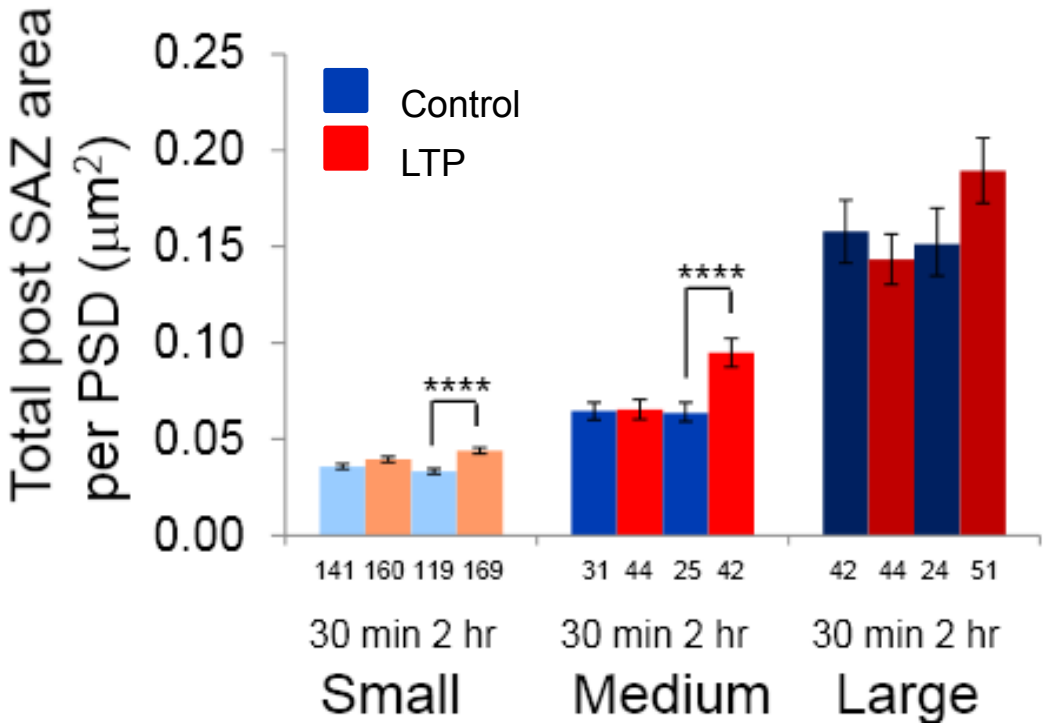

Figure 3.7 SAZ area at 30 min and 2 hr following LTP induction on all spine sizes. Control data is shown in shades of blue (light blue: small spine, medium blue: medium spine, dark blue: large spine.) LTP data is shown in shades of red (light red: small spine, medium red: medium spine, dark red: large spine). SAZ area remains unchanged on spines of all sizes at 30 min after LTP induction. SAZ area increases on small and medium spines only at 2 hr following LTP induction (n = number of PSDs). **** $P < 0.00001$.

Chapter 4

Presynaptic Enlargement

In Chapter 3, I demonstrated that by 2 hours following LTP induction, postsynaptic enlargement occurs via VFTZ growth. In this chapter, I will explore parallel changes in presynaptic vesicle counts and DCV distribution to identify the sequence of presynaptic events that occurs following LTP induction, and to determine whether these events precede or lag behind the postsynaptic changes.

4.1 A Decrease in Docked Vesicle Number at 30 minutes is Followed by Replenishment at 2 hours Following LTP Induction

I previously showed that VFTZ area decreased at 30 minutes and increased at 2 hours following LTP induction (see Fig. 3.6), and that VFTZ growth accounted entirely for PSD enlargement on large spines at 2 hours (see Fig. 3.7). One potential explanation is that vesicle release was enhanced by 30 minutes. The depleted docked vesicles were then replenished from non-docked vesicles closest to the presynaptic active zone by 2 hours. This depletion and replenishment occurred to a greater degree at large spines, thereby increasing the VFTZ area to a greater degree at 2 hours on those spines. To explore this possibility, it was necessary to differentiate between docked and non-docked vesicles at 30 minutes and 2 hours following LTP induction.

The structural definition of a docked vesicle requires its membrane to be in contact with the presynaptic membrane. Figure 4.1 shows a spine synapsing on an axonal bouton that contains a pool of non-docked vesicles (green arrow) and a vesicle that is docked at the presynaptic membrane (blue arrow). Previous

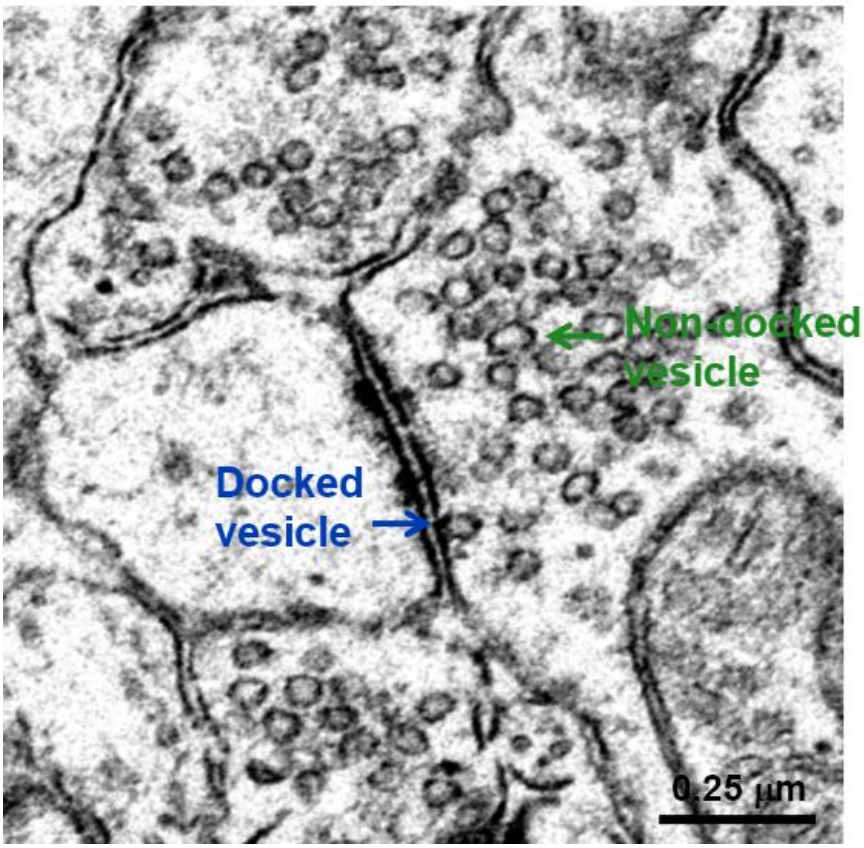

Figure 4.1 EM of a spine synapsing on an axonal bouton that contains a pool of non-docked vesicles (green arrow) and a docked vesicle (blue arrow) at the presynaptic membrane. Scale bar 0.25 μm.

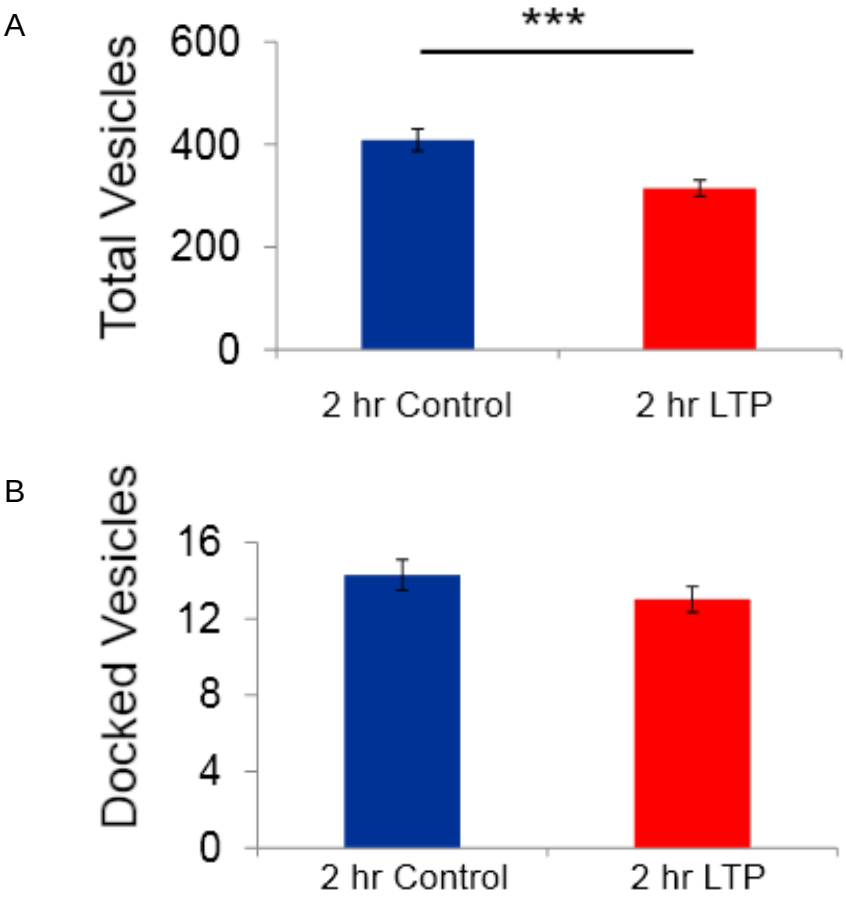

Figure 4.2 Vesicle counts at 2 hours following LTP induction. A) Total vesicle count (docked vesicles + non-docked vesicles) decreases at 2 hr following LTP induction. B) Docked vesicle count is unchanged at 2 hr following LTP induction relative to control (*** P <.0001)

work (Chirillo et al., 2009) measured changes in presynaptic vesicle counts at 2 hours following LTP induction and found that while the total number of vesicles was reduced in boutons synapsing on these enlarged synapses at 2 hours (Fig 4.2A), the number of docked vesicles was unchanged (Fig 4.2B). This finding may suggest that enhanced release had begun by 30 minutes and that docked vesicles were replenished from the non-docked vesicle pool by 2 hours, resulting in a reduction in the number of total vesicles.

I identified and stamped docked vesicles, those vesicles whose membranes were clearly in contact with the presynaptic membrane (Fig 4.1) in RECONSTRUCT™ (see Chapter 2), at each synapse included in the VFTZ analysis at 30 minutes and 2 hours following LTP induction in order to determine whether changes in VFTZ area corresponded to changes in the number of docked vesicles. I found that there were fewer docked vesicles at 30 minutes after LTP induction relative to control at synapses with medium and large spines, and that this decrease was greatest for large spines. There was no change in the number of docked vesicles 2 hours after LTP relative to control, suggesting that the depletion of docked vesicles observed at 30 minutes was followed by replenishment by 2 hours. There was an increase in the number of docked vesicles at 2 hours relative to 30 minutes, consistent with the creation of additional docking sites, which was also greatest for large spines. These results suggest that the depletion and replenishment of docked vesicles is greatest in boutons synapsing with large spines, requiring a greater depletion of non-docked vesicles close to the synapse, perhaps creating greater VFTZ area and the apparent lack of SAZ growth.

A

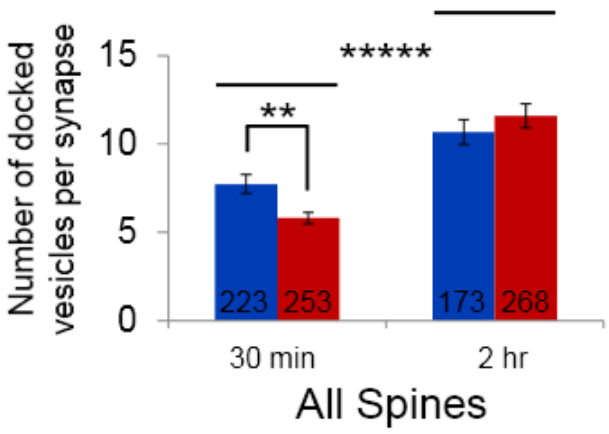

B

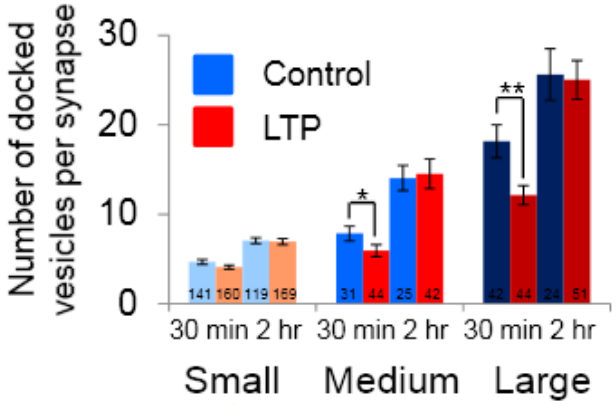

Figure 4.3 Docked vesicle counts at 30 minutes and 2 hours following LTP induction. A) Docked vesicle count for all spine types decreases at 30 min and returns to control level and increases relative to 30 min by 2 hr. B) Docked vesicle count decreases on medium and large spines at 30 minutes and returns to control levels and increases relative to 30 minutes on all spine sizes by 2 hr (light blue/red: small spine control/LTP, medium blue/red: medium spine control/LTP, dark blue/red: large spine control/LTP, n = number of synapses, * $P < 0.05$, ** $P < 0.001$, ***** $P < 0.000001$).

4.2 Small Presynaptic Dense Core Vesicles Serve to Enlarge the Presynaptic Active Zone Following LTP Induction

As discussed previously, active zone proteins are transported in the membranes of small presynaptic dense core vesicles (DCVs) that have a very densely stained core that is distinguishable from the vesicle membrane. It has also been demonstrated that there are fewer of these DCVs in axonal boutons following recuperative synaptogenesis in slice relative to perfused hippocampus (Fig 4.4,Sorra et al., 2006). This reduction could be due to the insertion of DCVs into axonal membranes to form the presynaptic active zones of new synapses. Additional work (Fig 4.5, Chirillo et al., 2009) has demonstrated that the fraction of axonal boutons that have DCVs increases 5 minutes after LTP induction relative to control. These additional DCVs could have been recruited to boutons in preparation for insertion to enlarge the presynaptic active zones of potentiated synapses. In these same experiments, spine number increased with time in vitro under control conditions by 2 hours in small spines (Fig 4.6, adapted from (Bourne and Harris, 2011a). I therefore analyzed DCV number at 30 minutes and 2 hours following LTP induction, with the hypothesis that DCV number decreases with time as spines proliferate in control and synapses enlarge in LTP conditions. This fraction is constant across condition at both 30 minutes and 2 hours for all spine types, indicating a return to control levels by 30 minutes consistent with DCV insertion at existing synapses between 5 and 30 minutes to enlarge the presynaptic active zone. However, the fraction of boutons containing DCVs at 2 hours was significantly reduced relative to 30 min for small and medium spines. Figure 4.8 shows the number of DCVs per bouton following LTP induction, which was unchanged relative to control at 30 min and 2 hours after LTP induction, but was significantly reduced for small and medium spines at 2

A

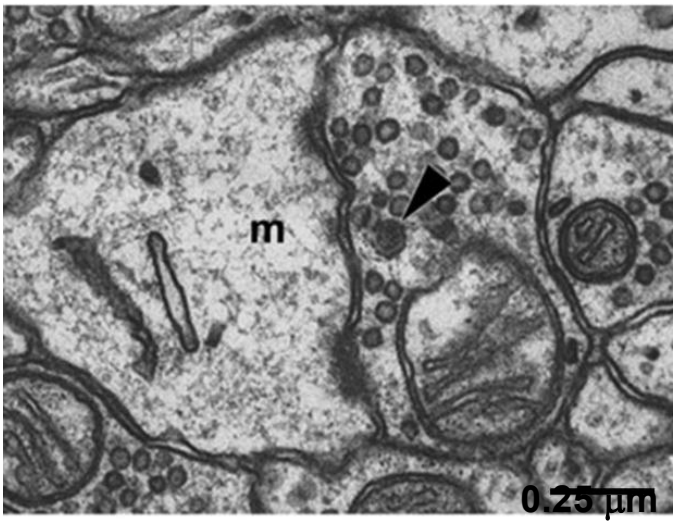

B

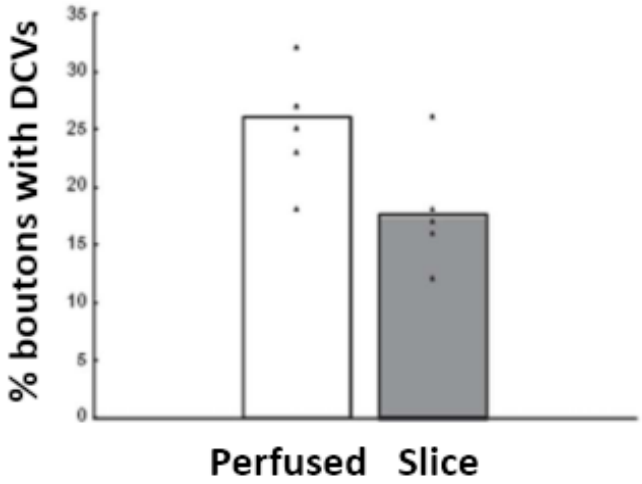

Figure 4.4 Dense core vesicles (DCVs) in hippocampal slices. A) Example DCV (arrowhead) in an axonal bouton. m = mushroom shaped large spine. B) Percentage of boutons containing DCVs is reduced in slice relative to perfused hippocampus (Figure from Sorra et al., 2006). Scale bar 0.25 µm

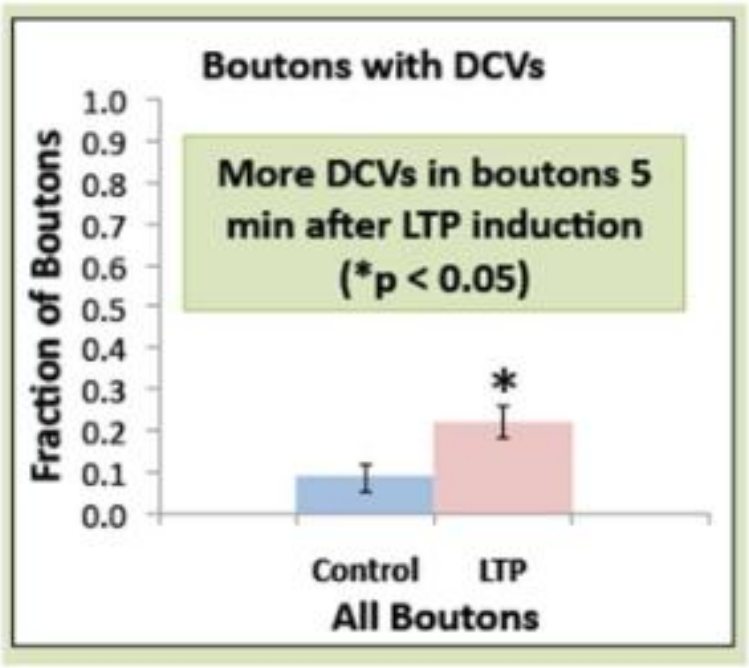

Figure 4.5 Fraction of boutons containing DCVs increases 5 minutes after LTP induction relative to control (Figure from Chirillo et al., 2009) (* P < 0.05).

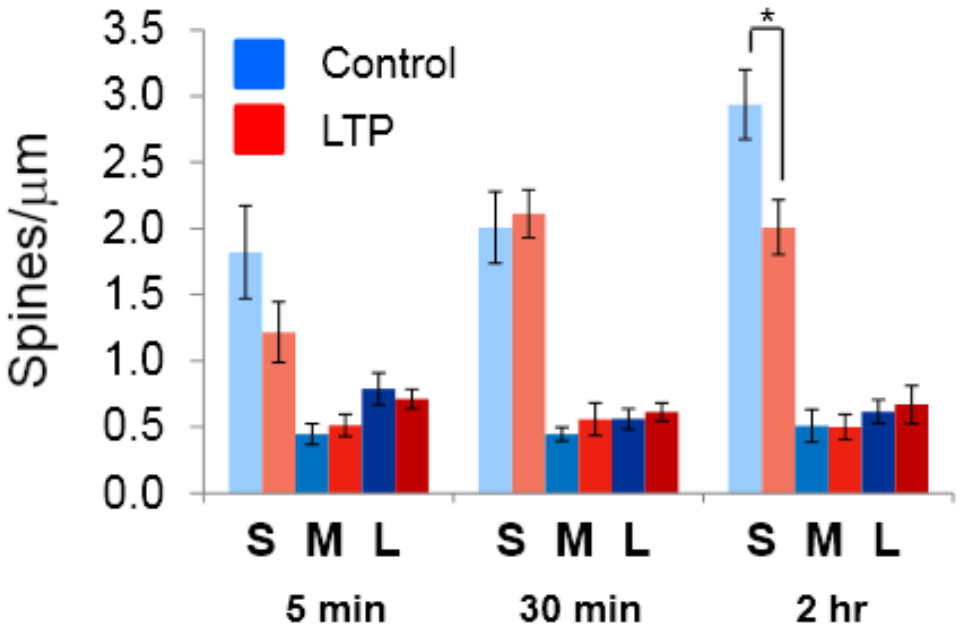

Figure 4.6 Spines per micron following LTP induction (light blue/red: small spine control/LTP, medium blue/red: medium spine control/LTP, dark blue/red: large spine control/LTP). Spine number increases with time in vitro under control conditions by 2 hr in small spines (* $P < 0.05$, figure modified from Bourne and Harris, 2011a).

LTP induction, but was significantly reduced for small and medium spines at 2 hours relative to 30 minutes.

Since there was no difference in DCV counts in the LTP condition relative to control, I collapsed the fraction of boutons containing DCVs and the number of DCVs per bouton across condition and compared across spine type (Fig. 4.9). The fraction of boutons containing DCVs was greater for large spines than small spines at 30 minutes and greater for large spines than small and medium spines at 2 hours after LTP induction. The number of DCVs per bouton was greater for large spines than small spines at 30 minutes and greater for large spines than for small and medium spines at 2 hours following LTP induction.

There is no LTP effect on DCV count at 30 minutes or 2 hours. However, there is a return to control levels at 30 minutes suggesting that the additional DCVs observed in the LTP condition at 5 minutes have been inserted at existing synapses to enlarge presynaptic active zones between 5 and 30 minutes. There is also a decrease in DCV count at small and medium spines between 30 minutes and 2 hours, which suggests that DCVs have been inserted at existing synapses to further enlarge their presynaptic active zones after LTP induction and to contribute to synaptogenesis during spine proliferation in the control condition during that time. That this effect is not present at large spines may indicate that presynaptic active zone assembly is delayed compared to that at synapses on small and medium spines because the degree of postsynaptic assembly is greater on large spines. The additional DCVs present at large spine synapses at 2 hours may be present for future incorporation into presynaptic active zones at their synapses, which could be determined in the future by looking at later time points after LTP induction. Docked vesicles are depleted the most at 30 minutes and replenished by much more at synapses on large spines by 2 hours following LTP induction, and large spines are more likely to be associated with presynaptic DCVs. It is therefore clear that large spines

A

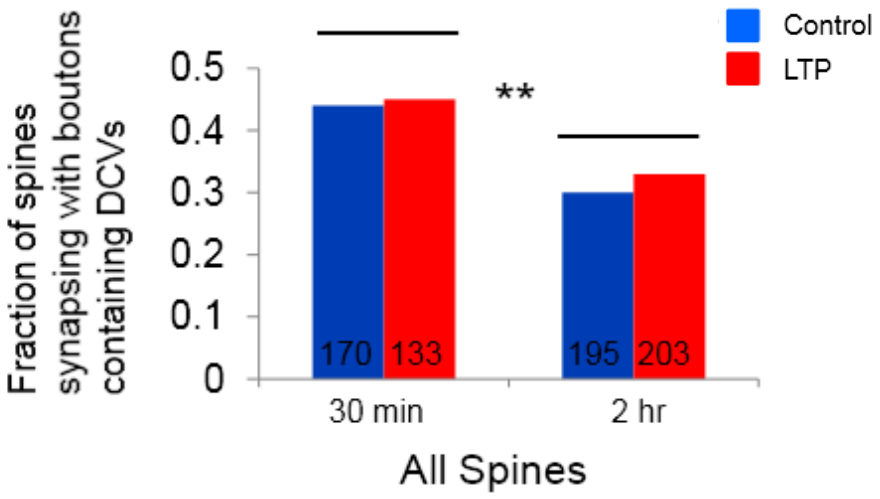

B

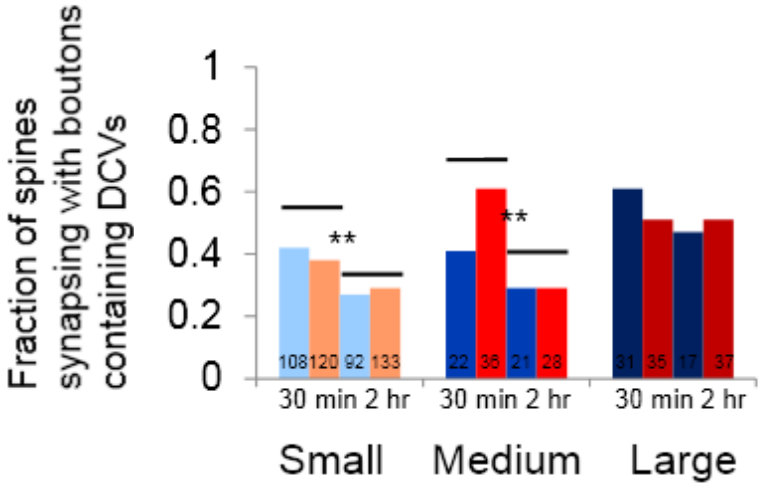

Figure 4.7 Fraction of spines synapsing with boutons containing DCVs. A) Fraction of all spines synapsing with boutons containing DCVs is unchanged relative to control at 30 min and 2 hr after LTP induction, but is significantly reduced at 2 hr relative to 30 min. B) Fraction of spines synapsing with boutons containing DCVs by spine type (light blue/red: small spine control/LTP, medium blue/red: medium spine control/LTP, dark blue/red: large spine control/LTP) The fraction of boutons containing DCVS at 2 hr is reduced relative to 30 min for small and medium spines(n = number of synapses, ** $P < 0.001$, chi-square).

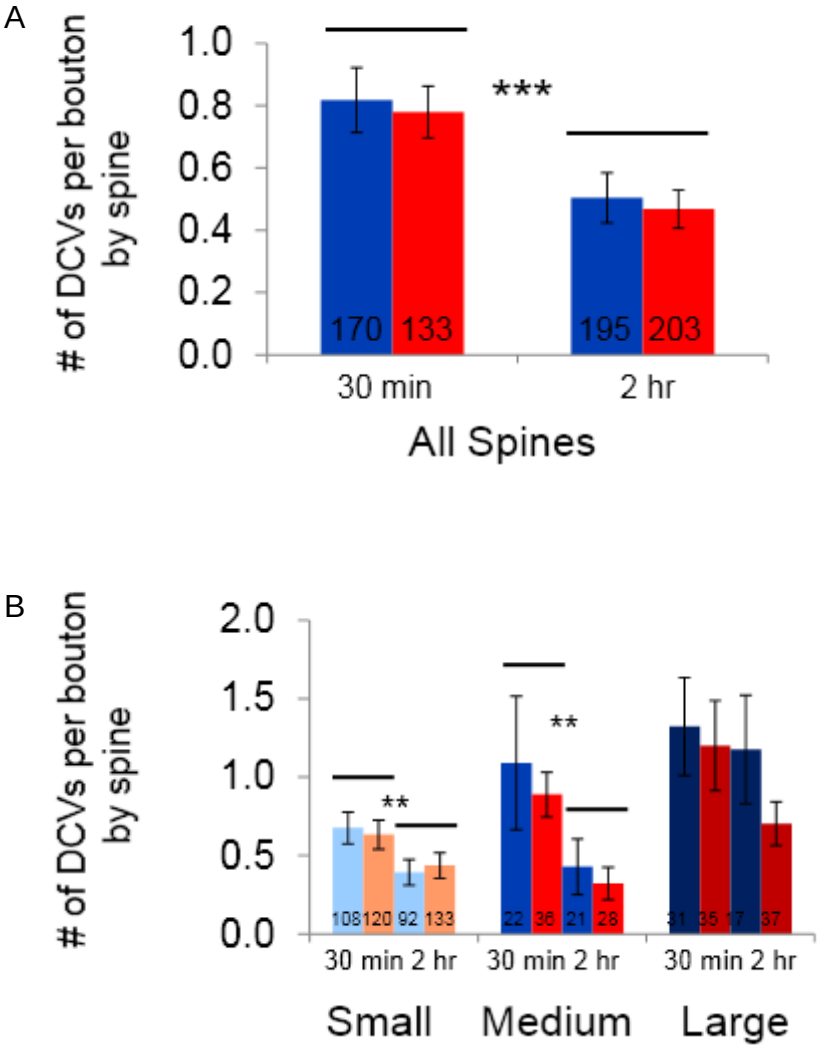

Figure 4.8 Number of DCVs per bouton. A) Number of DCVs per bouton is unchanged relative to control at 30 min and 2 hr after LTP induction, but is significantly reduced at 2 hr relative to 30 min. B) Number of DCVs per bouton by spine type (light blue/red: small spine control/LTP, medium blue/red: medium spine control/LTP, dark blue/red: large spine control/LTP) The fraction of boutons containing DCVS at 2 hr is reduced relative to 30 min for small and medium spines(n = number of synapses, ** $P < 0.001$, *** $P < 0.0001$).

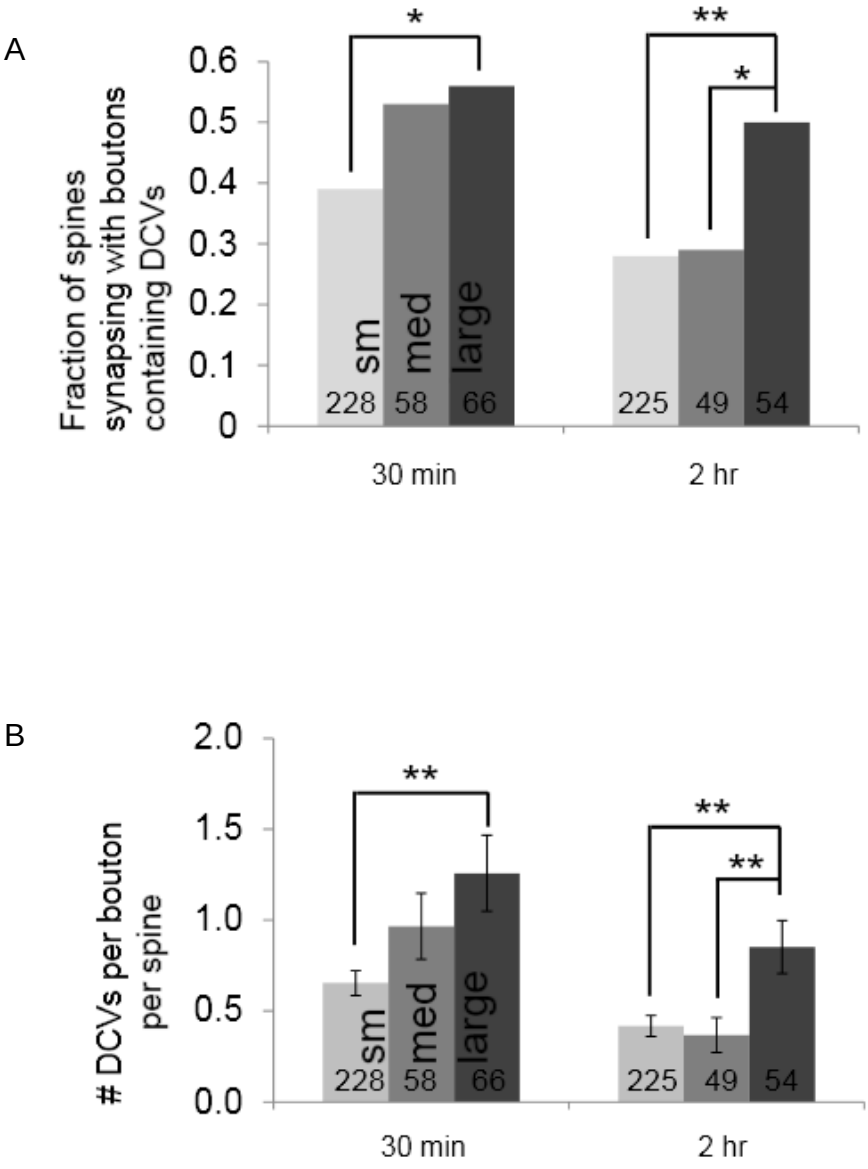

Figure 4.9 DCV frequency by spine type. A) Fraction of boutons with DCVs is greater for large spines at 30 min and 2 hr after LTP induction. B) Number of DCVs per bouton is greater for large spines at 30 min and 2 hr (n = number of synapses, * $P < 0.05$, ** $P < 0.001$).

command more of both the presynaptic assets necessary for synapse growth, which may help account for the loss of small spines seen at 2 hours after LTP induction (Figure 4.6), as some of them are out-competed for resources by their larger counterparts.

Chapter 5

Discussion

This study examined pre- and postsynaptic structural changes in mature hippocampal area CA1 during LTP. Changes in VFTZ frequency and size, DCV frequency, and vesicle redistribution were observed. Each of these synaptic elements contributed to synapse enlargement, which was accomplished by a redistribution of synaptic resources.

5.1 VFTZs, DCVs, and docked vesicles enlarge synapses during LTP

Figure 5.1 illustrates the pre- and postsynaptic structural changes that occur following LTP induction. By 5 minutes, the DCV count in the LTP condition is elevated relative to control, suggesting a recruitment of additional DCVs to axonal boutons in preparation for insertion at existing synapses to enlarge their active zones.

By 30 minutes, DCV levels return to control, indicating that the additional DCVs present at 5 minutes were inserted by 30 minutes. There is also a reduction in VFTZ area (on small and large spines), suggesting that by 30 minutes, additional vesicles had been recruited to existing VFTZs but had not yet docked, as PSD area did not increase by 30 minutes (Bourne and Harris, 2011a). There was also an decrease in docked vesicle count (on spines of all sizes) at 30 minutes. The decrease in docked vesicle count could be due to increased release due to stimulation or due to delayed recycling of released vesicles following LTP induction. A possible explanation for delayed recycling involves the increase in DCV number relative to control at 5 minutes after LTP induction (Fig 4.5), which returned to control levels by 30 minutes (Fig. 4.7). It could be that the additional DCVs that were recruited to axonal boutons at 5 minutes were subsequently inserted into the presynaptic membranes at the edges of existing

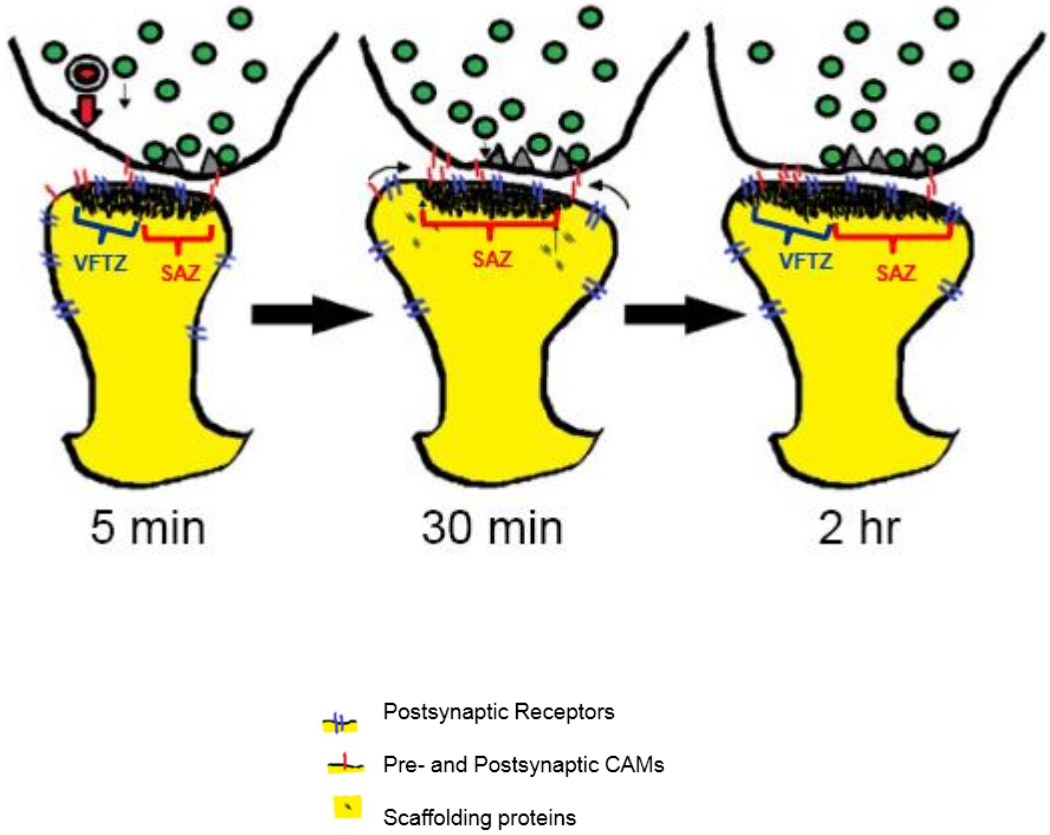

Figure 5.1 Structural sequence of events and model of synapse enlargement. At 5 min during LTP, DCVs are inserted opposite VFTZs at existing synapses and insert CAMs into cleft. These CAMs bind their partners in the VFTZ, recruiting presynaptic vesicles to existing VFTZs, reducing VFTZ area by 30 min. Simultaneously, glutamate receptors in the perisynaptic region and cytoplasmic scaffolding proteins are recruited to the edges of existing PSDs to begin to assemble VFTZs. By 2 hr, the VFTZs have been assembled and are visible by EM. SAZ area is also increased on small and medium spines, but VFTZ increase accounts for PSD enlargement on large spines. The increase postsynaptic response observed at 2 hr may be due to the response of AMPA receptors in new VFTZs to increased glutamate spillover from the SAZ.

synapses, annexing recycling zones adjacent to presynaptic active zones in the process.

By 2 hours, VFTZ growth contributed to PSD growth on spines of all sizes. On small and medium spines, SAZs also grew, indicating that additional vesicles mobilized to VFTZs on these spines, but VFTZs account for the entire growth of large spine PSDs. There was also an increase in the number of docked vesicles at spines of all sizes at 2 hours. This increase suggests a replenishment, possibly from the non-docked vesicle pool, at 2 hours of the depletion of docked vesicles at 30 minutes. Synapses on large spines experienced a greater depletion of docked vesicles by 30 minutes followed by a greater replenishment of docked vesicles by 2 hours. This replenishment could be achieved by the recruitment of more non-docked vesicles close to the SAZ to new or existing docking sites, perhaps resulting in greater VFTZ area. This increase (in medium and large spines) and replenishment (in all spine types) in docked vesicles may allow for enhanced LTP-dependent sustained release. The increase in VFTZ area could account for enhanced postsynaptic response. Finally, dense core vesicle count decreased by 2 hours relative to 30 minutes, possibly to support ongoing spine formation in the control condition and synapse enlargement following LTP induction. That this decrease is not observed for large spines may indicate that the greater degree of postsynaptic assembly required of these spines delayed presynaptic assembly with respect to their smaller counterparts. Such a delay could also account for the fact that SAZ size also did not change by two hours on large spines as well, as follows. DCV insertion at 5 minutes preceded vesicle recruitment at 30 minutes. This may be a recurring cycle, with multiple waves of DCV insertion preceding additional vesicle recruitment. Additional DCVs may have been inserted to enlarge the presynaptic active zones on small and large spines between 30 minutes and 2 hours, resulting in vesicle recruitment to VFTZs, enlarging the SAZs by 2 hours. These additional dense core vesicles may be inserted at existing synapses on large spines at some point

after 2 hours, as the degree of postsynaptic assembly is greater for large spines. It would be interesting to look at later time points to see if DCVs are inserted at large spines after 2 hours, and if their insertion precedes another wave of vesicle recruitment.

5.2 Balancing synaptic resources

Large spine synapses were more likely to have more and larger VFTZs, to be associated with boutons containing more DCVs, and to experience greater depletion of docked vesicles at 30 minutes and greater replenishment from non-docked pool at 2 hours following LTP induction. In other words, large spines command more of both pre-and postsynaptic resources necessary for synapse enlargement than their smaller counterparts. This evidence for a coordinated balance of synaptic inputs is consistent with other recent findings. At 5 minutes after LTP induction there was an increase in polyribosomes in large spines (Bourne and Harris, 2011b). Furthermore, at 2 hours after LTP induction, there was a redistribution of polyribosomes from the dendritic shaft to spines with large PSDs in both developing and mature hippocampus (Bourne et al., 2007;Ostroff et al., 2002), and only spines with enlarged PSDs contained polyribosomes (Bourne and Harris, 2011a). Together these results suggest that synaptic plasticity is coordinated across multiple dendritic spines and their presynaptic partners in order to maintain a balance of synaptic activity.

5.3 Assembly of presynaptic active zone is unitary

It has been suggested that DCVs serve as ‘active zone precursor vesicles’ that could allow for the formation of new active zones by fusing with the presynaptic plasma membrane. Quantitative analysis demonstrated that the amount of bassoon, piccolo and Rim present in presynaptic boutons corresponded to integer multiples of the amount of bassoon, piccolo and Rim

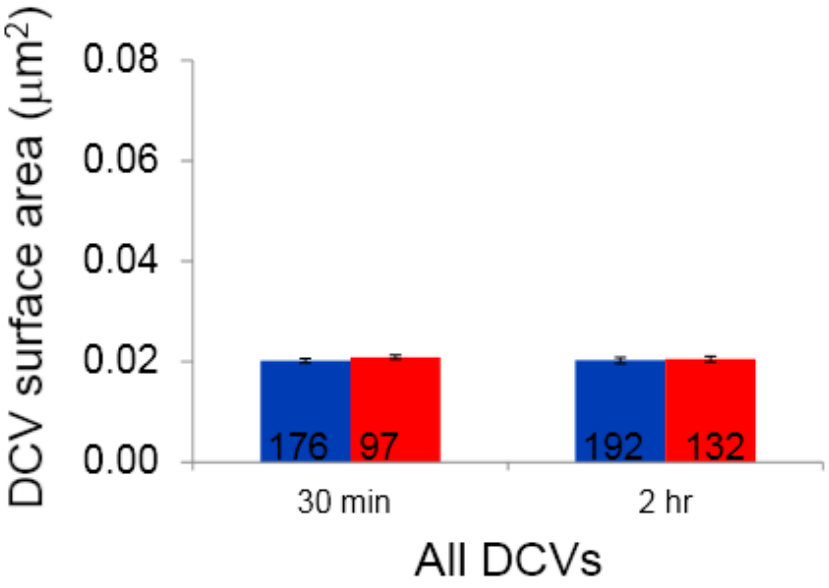

Figure 5.2 DCV diameters are consistent across condition and time point, resulting in comparable surface areas (n = number of DCVs).

	2 HR CTRL MIN	2 HR LTP MIN	2 HR CTRL AVG	2 HR LTP AVG	Δ	# CTRL MIN NEEDED TO ENLARGE SAZ	# CTRL MIN NEEDED TO ENLARGE SAZ	# CTRL AVG NEEDED TO ENLARGE SAZ	# LTP AVG NEEDED TO ENLARGE SAZ	# Δ NEEDED TO ENLARGE SAZ
SAZ	-	-	0.0054 μm^2	0.08 μm^2	0.026 μm^2	-	-	-	-	-
VFTZ	0.0034 μm^2	0.0053 μm^2	0.009 μm^2	0.014 μm^2	0.005 μm^2	~ 8	~ 5	~ 3	~ 2	~ 5
DCV	-	-	0.02 μm^2	0.02 μm^2	0 μm^2	-	-	~ 1	~ 1	-

Table 5.1 SAZ, VFTZ, and DCV areas and changes in areas are compared.

transported by DCVs, indicating that the DCV may serve as the unit of presynaptic active zone assembly (Shapira et al., 2003). Time-lapse imaging of DCVs labeled for bassoon demonstrated rapid axonal transport (Shapira et al., 2003) and the creation new functional active zones. The area of these new active zones corresponded to the recruitment of 2–5 DCVs to these sites (Bresler et al., 2004;Shapira et al., 2003).

The results of this study indicate that they may also be the means by which presynaptic active zones enlarge at growing synapses. DCV diameters are tightly distributed, resulting in very consistent surface areas across condition and time point (Fig. 5.2). The postsynaptic active zone (SAZ in Table 5.1) is the portion of the PSD that apposes the presynaptic region that contains vesicles, and is therefore likely a functional presynaptic active zone. The area by which the postsynaptic active zone expands would then correspond to the area by which the presynaptic zone expands. Table 5.1 compares the mean DCV surface area to the mean change in postsynaptic active zone area. The mean area by which the postsynaptic active zone grew corresponds roughly to the surface area of 1 DCV. This is a reasonable area by which the presynaptic active zone might expand by 2 hours following LTP induction, which is consistent with the role of the DCV as the presynaptic unit of synaptic growth.

5.4 VFTZs and increase in AMPARs during LTP

If VFTZs are the unit of presynaptic growth, which correlates with enhancement of postsynaptic response, it is probable that they contain AMPA receptors. AMPARs mediate fast synaptic transmission at excitatory synapses, and their accumulation within synapses is important for enhanced transmission during LTP (Bredt and Nicoll, 2003;Malinow and Malenka, 2002;Collingridge et al., 2004;Shepherd and Huganir, 2007; Sheng et al., 2002). Multiple studies have examined the role of both AMPAR removal and insertion at the synapse during

	2 HR CTRL MIN	2 HR LTP MIN	2 HR CTRL AVG	2 HR LTP AVG	D
VFTZ	0.0034 μm^2	0.0053 μm^2	0.009 μm^2	0.014 μm^2	0.005 μm^2
# 50 nm vesicles needed	~ 0.4	~ 0.7	~1	~2	~ 0.6

	2 HR CTRL AVG	2 HR LTP AVG	D
SAZ	0.0054 μm^2	0.08 μm^2	0.026 μm^2
# 50 nm vesicles needed	~ 0.7	~10	~ 3

Table 5.2 SAZ, VFTZ, and 50 nm postsynaptic AMPAR-containing vesicle areas are compared.

synaptic plasticity. The application of glutamate to hippocampal cultures resulted in an extreme reduction in synaptic AMPARs but not NDMARs over a time span that is comparable to that of LTD expression (Lissin et al., 1999), and the activation of AMPARs, NMDARs, insulin receptors and metabotropic glutamate receptors can result in the rapid reduction of synaptic AMPARs as a result of internalization from the membrane surface (Carroll et al., 1999;Zhou et al., 2001;Beattie et al., 2000;Man et al., 2000;Ehlers, 2000; Snyder et al., 2000). Conversely, the increase in synaptic strength during LTP is mediated by insertion of AMPARs into the synaptic membrane. NMDAR activation induces spinogenesis in hippocampal slices (Svoboda and Mainen, 1999) and recruits AMPARs to the plasma membrane (Fischer et al., 2000), which stabilize and maintain dendritic spines (Malinow and Malenka, 2002;McKinney et al., 1999). For example, blocking interactions with the C-terminus of GluR2 in postsynaptic cells prevented the potentiation of silent synapses, which contain NMDA, but not AMPA, receptors in spinal neurons (Li et al., 1999). In imaging studies of GFP-tagged AMPAR subunit GluR1, GluR1 redistributed into synaptic spines following LTP induction in cultured hippocampal slices (Shi et al., 1999). Additionally, an increase in synaptic AMPAR mediated currents was detected in cultured hippocampal neurons following the application of glycine, an NMDAR co-agonist, as well as an increase in synaptic AMPAR surface expression (Lu et al., 2001). The same study also demonstrated, using immunocytochemical labeling for only newly inserted AMPARs, an increase in the delivery of AMPARs to synapses. Therefore, it seems likely that VFTZs observed at two hours contain AMPARs, as increased postsynaptic response would depend in part upon an increase in AMPAR response at the synapse.

5.5 Unitary versus continuous assembly of PSDs and VFTZs

There has been speculation that PSDs are assembled in a unitary manner as well. Structural evidence for exocytosis was observed in spines in CA1, where

~ 50 nm smooth vesicles were found fusing with plasma membrane in spine heads in CA1 (Spacek and Harris, 1997; Cooney et al., 2002). Changes in synapse strength can result from fusion of this type of transport vesicle carrying new membrane material to the spine membrane (Lledo et al., 1995, Park et al., 2006). Furthermore, membrane fusion inhibitors blocked LTP in CA1 pyramidal cells (Lledo et al., 1995). In addition to membrane transport, vesicles in spines have been shown to transport synaptic receptors, including AMPA-type glutamate receptors (Sans et al., 2003;Washbourne et al., 2004). AMPARs are typically concentrated at the edges of the PSD, where VFTZs are found, or homogeneously distributed throughout the PSD (Masugi-Tokita et al., 2007). AMPAR GLu-R1 subunit-containing vesicles have been observed associating with the cytoplasmic side of GluR1-containing synapses (Kharazia et al., 1996).

Because 1) AMPARs are frequently localized to regions at the edges of synapses, and therefore possibly VFTZs, 2) AMPARs are transported in 50 nm vesicles that associate with the PSD, and 3) insertion of additional AMPARs at the synapse contributes to the increase in synaptic strength during LTP, it is possible that 50 nm AMPAR-transporting vesicles at the synapse are the source of a portion of the material required for VFTZ assembly, in which case VFTZ area and SAZ area could be multiples of the surface area of these 50 nm vesicles, which is roughly of 0.0079 μm^2. In other words, if PSD growth is facilitated by the insertion of 50 nm AMPAR-containing vesicles, they may serve as the postsynaptic analog of DCVs in the presynaptic cell. While DCVs transport materials necessary for expansion of the presynaptic active zone, these postsynaptic vesicles may transport receptors to build or expand VFTZs at existing synapses following LTP induction. Table 5.2 compares the surface area of 50 nm postsynaptic AMPAR-containing vesicles (0.0079 μm^2) to VFTZ and SAZ areas. Because the minimum VFTZ areas are much smaller than the vesicle surface area, it seems unlikely that newly created VFTZs would be generated by the insertion of AMPAR-containing vesicles directly at the synapse. On the other

hand, additional vesicles have been recruited to VFTZs on small and medium spines by 2 hours after LTP induction, enlarging the SAZs and decreasing VFTZ area. It could be that the insertion of AMPAR-containing vesicles to create or enlarge VFTZs at potentiated synapses was followed closely by vesicle recruitment, and that another time point(s) between 30 minutes and 2 hours after LTP induction would capture that sequence of events.

Table 5.1 also compares the minimum VFTZ surface area, mean VFTZ surface area, and the change in mean VFTZ area to the change in mean SAZ area between control and LTP conditions at 2 hours after LTP induction. The mean area by which the postsynaptic active zone grows corresponds roughly to the area of 8 x that of the smallest control VFTZ and 5 x that of the smallest LTP VFTZ. The mean area by which the postsynaptic active zone grows corresponds roughly to the area of 3 x that of the mean control VFTZ and 2 x that of the mean LTP VFTZ. The mean area by which the postsynaptic active zone grows corresponds roughly to the area of 5 x that of the difference between the mean LTP VFTZ and the mean control VFTZ. Unlike DCV surface area, individual VFTZ area is not normally distributed (Fig. 5.3), so the “peakiness” of the VFTZ and SAZ area distributions was examined to determine which, if any, of these quantities could serve as a unit of postsynaptic expansion following LTP induction. In order to determine the mean quantal amplitude, or the postsynaptic response to the presynaptic release of a single quantum of neurotransmitter, quantal analyses of the distribution of peak EPSPs from postsynaptic partners of neurotransmitter-releasing boutons were examined (Jack et al., 1994;Lisman and Harris, 1993). These distributions had multiple and evenly spaced peaks corresponding to the release of integer multiples of one quantum of neurotransmitter. In order to determine if the VFTZ areas are distributed similarly, meaning, if there is a fundamental minimal unit of VFTZ assembly, VFTZ distributions at 2 hours following LTP induction were examined to determine if evenly spaced peaks were present. Figure 5.3 shows the distribution of individual

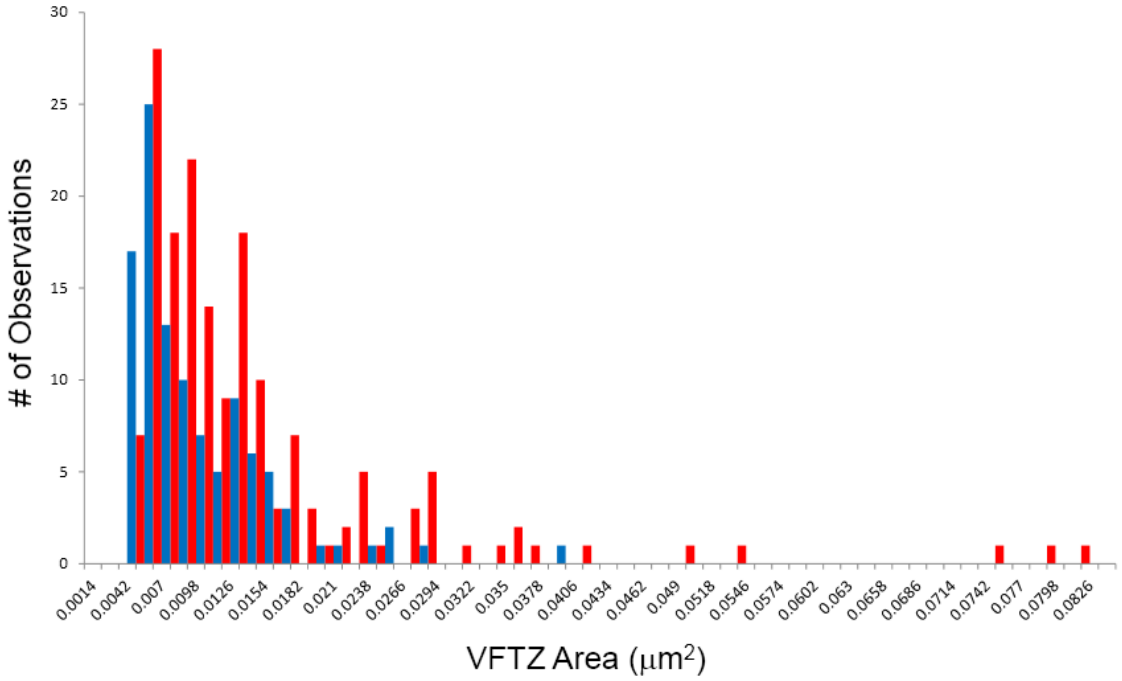

Figure 5.3 Individual VFTZ areas (μm^2) for control (blue) and LTP (red) at 2 hours following LTP induction. Both distributions show peaks, but peaks are not evenly spaced.

VFTZ areas in control (blue) and LTP (red) conditions at 2 hours. Each distribution has discernable peaks at multiple locations, but they are not evenly spaced. Furthermore, the spacing between the peaks in the LTP condition is less than the surface area of the putative transport vesicle (0.0079 μm^2). I also looked for evenly spaced peaks at multiple frequencies in the SAZ area distribution at 2 hours following LTP induction. Figure 5.4 shows the distribution of SAZ areas in control (blue) and LTP (red) conditions at 2 hours following LTP induction. Each distribution shows only one obvious peak; if the SAZ were composed of unit regions corresponding to the insertion of postsynaptic vesicles at the postsynaptic site, then one would expect the distribution of areas to show peaks corresponding to multiples of the vesicle surface area. Based on the distributions of both VFTZs and SAZ area in control and LTP conditions, this study provides no evidence that VFTZs or SAZs are created in a unitary fashion by insertion of AMPAR-containing vesicles at the PSD.

5.6 Lateral diffusion of AMPARs and synapse enlargement

Previous work has also provided evidence suggesting that PSD enlargement most likely does not occur through the direct insertion of discrete packets of postsynaptic proteins at the synapse itself. Synaptic activity has been shown to alter the rate of AMPA receptor diffusion through membrane trafficking (Borgdorff and Choquet, 2002;Tardin et al., 2003;Groc et al., 2004). NMDAR activation triggers the exocytosis of AMPARs mainly to extra- and perisynaptic sites (Kennedy et al. 2010;Lin et al., 2009;Passafaro et al., 2001;Yudowski et al., 2007). By 5 minutes after chemical LTP induction, the percentage of mobile synaptic GluR2 AMPA receptors increased but returned to baseline levels after 40 minutes. This suggests that newly recruited synaptic GluR2 receptors are mobile immediately after LTP induction, but stabilize fairly quickly (Tardin et al., 2003). These results are consistent with FRAP experiments that demonstrated

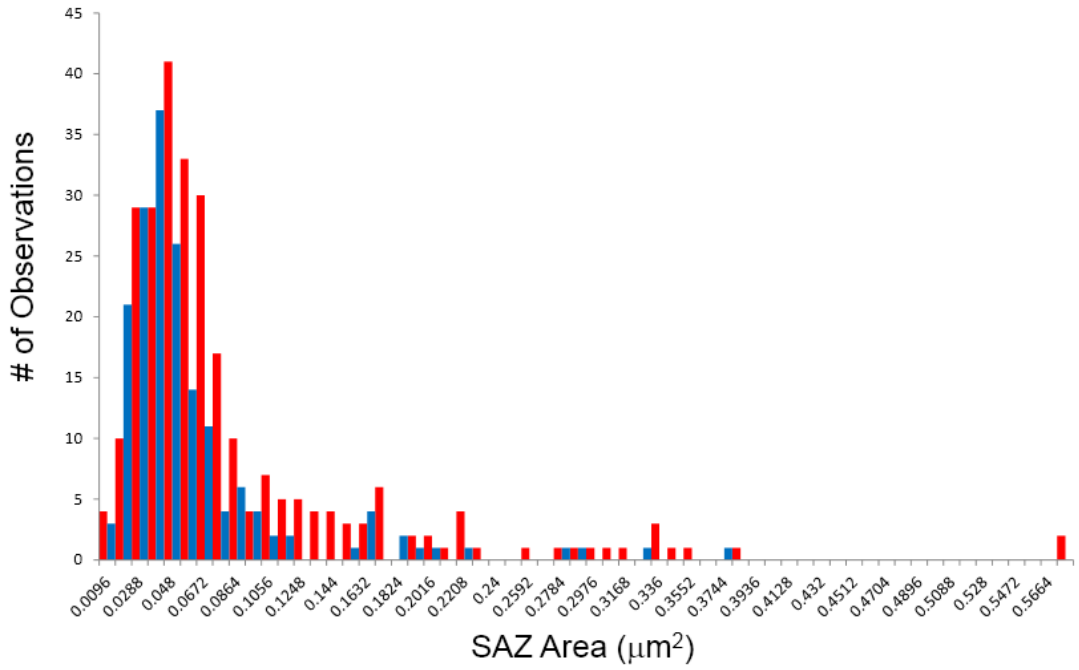

Figure 5.4 SAZ areas (μm^2) for control (blue) and LTP (red) at 2 hours following LTP induction. Each distribution has only one peak.

that chemical LTP stimuli increased exchangeable EYFP-GluR1 in spines but decreased the recovery rate post-photobleaching (Sharma et al., 2006). These data suggest that while more GluR1 AMPA receptors are mobile, fewer synaptic receptors are being exchanged, which indicates synaptic trapping of AMPA receptors. Membrane GluR2-containing AMPARs experience reversible periods of immobilization that increase in both frequency and duration in young neurons in parallel with synaptogenesis (Borgdorff, 2002). Regions of receptor confinement were associated with synaptic structures, demonstrating a region of low receptor diffusion around synapses that could correspond to reversible integration of additional AMPA receptors at the edge of the PSD (Nusser, 2000).

The region a distance of ~ 100 – 200 nm from the PSD edge has been loosely defined as the “perisynaptic” region. GluR2-containing AMPARs move from the PSD into the perisynaptic domain when a glutamate bath is applied, and the number of perisynaptic GluR2 receptors decreases following chemical LTP induction (Tardin et al., 2003, 2001;Luscher et al., 1999). These results suggest that the perisynaptic pool of AMPA receptors serves as a source of additional receptors for the PSD. There is also evidence that the majority of mobile AMPARs diffuse laterally along the spine membrane from extrasynaptic regions (Makino and Malinow, 2009). In addition, the loss of extrasynaptic AMPARs precedes synaptic receptor loss upon NMDAR activation (Ashby et al., 2004;Isaac et al., 2007). This indicates that the perisynaptic region may serve as a region through which AMPARs are trafficked between the PSD and extrasynaptic region, and in which AMPARs can be held in reserve. Furthermore, the rate of exchange by lateral diffusion is more rapid than that by exocytosis. When lateral diffusion is prevented by cross-linking surface AMPARs, constitutive exocytosis does not create a recovery from photobleaching over the time course of a typical FRAP experiment (Ashby et al., 2006). This is consistent with previous results suggesting that lateral diffusion is more rapid than transport from

inside the cell (Adesnik et al., 2005). The mean $t_{1/2}$ of the FRAP for AMPARs in spine heads was 222.7 s, which indicates that the mobile population of spine AMPARs is almost completely exchanged in ~15–20 min. These numbers are more consistent with the time course of synapse enlargement following LTP induction than the slower AMPAR exocytosis. Following synaptic potentiation, most AMPAR exocytosis does occur on dendrites and may serve to replenish the local extrasynaptic pool (Makino and Malinow, 2009), indicating that lateral movement of AMPARs along plasma membranes at the local level allows for synapse enlargement, and that homeostasis on the dendritic level may be mediated in part by the exocytotic system that supplies these receptor populations.

Quantum dot studies, which employed the silencing of individual presynaptic boutons, have demonstrated that local synaptic activity reduces lateral exchange of GluR1 between synaptic and extraynaptic regions and an accumulation of GluR1 at the synapse (Ehlers et al., 2007). Furthermore, GluR1 is highly mobile at nearby inactive synapses, where receptors frequently escape to the extrasynaptic region. More recent quantum dot studies have found an inverse correlation between AMPAR diffusion and NLG-1 expression level, which depended upon the GLUR2 subunit and intact Nlg1/PSD-95 interactions (Mondin et al., 2011). Decrease in AMPAR mobility may be due to an increase in PSD-95 clusters, which trap AMPARs at the synapse through the phosphorylation of auxiliary subunit stargazin by CAMKII (Opazo et al., 2010). Furthermore, nrx-1 assembled NLG-1/PSD-95 clusters to which functional AMPARs were recruited within 1 h, which required AMPAR membrane diffusion (Mondin et al., 2011). The formation of these new neurexin/neuroligin adhesions also caused a depletion of PSD-95 from existing synapses and a drop in their AMPAR responses. These results suggest that neurexin/neuroligin interactions trigger the simultaneous trafficking of cytoplasmic PSD-95 and AMPA receptors in the peri/extrasynaptic region to the synapse and a decrease in synaptic AMPAR mobility to prevent

synaptic AMPAR loss following synaptic activity. This is counterbalanced by a loss of AMPARs and PSD-95 from neighboring inactive synapses, reflecting the same homeostatic regulation observed following LTP induction (Bourne and Harris, 2011a).

5.7 Modular organization of functional synaptic units

Even if VFTZs are indeed AMPAR-containing expansions of the PSD, the AMPARs are not necessarily positioned in such a way as to be activated by glutamate release from the presynaptic active zone. Vesicles docked at the presynaptic membrane release glutamate into the cleft following stimulation through the creation and opening of a fusion pore, whose diameter determines how rapidly glutamate enters the cleft. The current due to the opening of the smallest pore would be on the order of noise and would be impossible to detect, creating a 'whispering' form of silent synapse. Once released, glutamate (at an initial concentration within the vesicle of 200 mM; Tanaka et al., 2005) passes through the pore and diffuses once in the cleft, at a rate only marginally slower than free diffusion (Nielsen et al., 2004) and binds postsynaptic AMPA receptors (at a density of ~1,000 per μm^2;Tanaka et al., 2005). The fast, controlled application of glutamate to excised outside-out patches showed that micromolar levels of glutamate can bind to single AMPAR subunits, causing the receptor to adopt a long-lived desensitized state without opening (Magee and Cook, 2000). However millimolar levels of glutamate induce rapid channel opening followed by desensitization, therefore the more glutamate that binds, the greater the probability of channel opening before desensitization. Computer simulations indicate that glutamate levels in the cleft peak at ~80 μs following release and demonstrate a large concentration gradient (Raghavachari and Lisman, 2004). Only receptors within ~100 nm of the release site are exposed to the millimolar concentration necessary for activation, which corresponds roughly to the minimum area of a VFTZ. Glutamate binds to postsynaptic AMPARs mainly

within that region (area ~ 0.03 μm^2, which is only ~25% of the area of the average CA1 synapse), in ~10 μs, and open conformation occurs in ~100 μs. These results are consistent with previous evidence that the average quantal current does not saturate (Silver et al., 1996;Liu et al., 1999;McAllister and Stevens, 2000). Therefore it is AMPAR density rather than AMPAR number that determines quantal size (Raghavachari and Lisman, 2004;Franks et al., 2002) at the synapse. However, AMPARs in additional VFTZs at 2 hours that are within ~100 nm of the edge of the SAZ can be activated in response to increased glutamate spillover from the SAZ, increasing postsynaptic response during LTP.

On the other hand, the majority of VFTZ area (i.e. that not immediately adjacent to the PSD) may represent a functionally as well as structurally distinct region of the PSD. Silent synapses, which contain only NMDA-type glutamate receptors, can accumulate AMPA receptors in an activity-dependent manner (Durand et al., 1996;Isaac et al., 1995; Liao et al., 1995, 1999;Petralia et al., 1999). Uncaging glutamate on new spines elicits mEPSC amplitude rise times consistent with the presence of AMPARs, and the response was comparable to that of mature spines of similar sizes (Zito et al., 2009). Even very new spines showed AMPAR responses, which increased as spines grew, and many formed synapses within a few hours. However, some synapses on spines of all sizes had responses on the order of noise, suggesting that spines of all sizes have synapses that go through a brief “silent phase” (Zito et al.,2009). Therefore, synapses need not be categorically “silent” or completely functional. Functional synapses may be modular, and some of them may be “partially silent”; they may be composed of both AMPA-silent and AMPA-functional modules. AMPA silent modules would release presynaptic glutamate slowly (causing immediate AMPAR desensitization) and/or and lack postsynaptic AMPA receptors, whereas AMPA-functional modules would contain AMPA receptors and release glutamate rapidly or respond to spillover. For example, inhibiting desensitization with cyclothiazide dramatically increases AMPAR-mediated EPSCs without affecting

the amount of glutamate released (Choi et al.2000), suggesting the slowly released glutamate in AMPAR-silent modules can activate AMPARs that were previously desensitized (Raghavachari and Lisman, 2004;Lisman and Raghavachari, 2006). Furthermore, application of low affinity antagonist demonstrates decreased reduction in the EPSC after LTP induction than before LTP (Choi et al., 2000), indicating an increased glutamate concentration in the synaptic cleft after LTP. The number of vesicles released (measured by NMDAR-mediated EPSCs) was unchanged, therefore LTP likely increased the fusion pore diameters of releasing vesicles, resulting in a more rapid release of glutamate and decreased desensitization of AMPARs. Therefore, in theory, LTP could both add AMPA channels and increases the fusion pore diameter in silent modules at existing synapses, making them functional. At the same time, there may be a corresponding decrease in functional modules in neighboring synapses that were not potentiated, resulting in an overall balance in the total functional postsynaptic area. The ratio of total VFTZ area to total PSD area is maintained across both spine type and condition (Fig 5.5), similar to the way that total PSD area is maintained. The consistency of this ratio suggests that the insertion of additional VFTZ at enlarging synapses creates additional functional modules by adding AMPA receptors that can respond to increased glutamate concentration in the synaptic cleft following LTP. This increase is balanced by the removal of AMPAR-containing VFTZ at unpotentiated synapses, reducing AMPA functional modules in order to maintain an overall balance of synaptic resources along dendritic segments. Saturation of LTP may occur at the point at which no additional resources can be recruited to potentiated synapses from nearby synapses without disrupting the circuits in which those nearby synapses are involved. Small VFTZs would possibly be present at synapses at which LTP has saturated, as they could respond to enhanced glutamate spillover from the active zone, but large VFTZs would seem unlikely, as AMPA receptors located far from

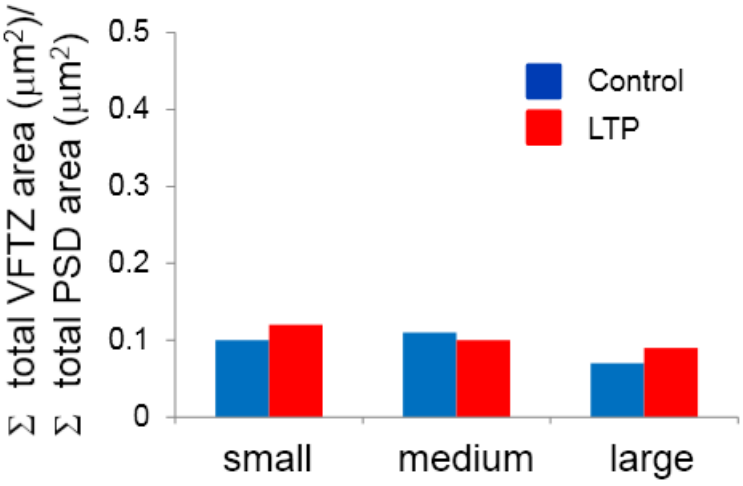

Figure 5.5 Ratio of total VFTZ area (μm^2) to PSD area (μm^2) for control (blue) and LTP (red) at 2 hours following LTP induction for each spine size. Ratio is constant across condition and spine type, suggesting a balance of functional postsynaptic area across dendritic segments following LTP induction.

the synaptic active zone would not be activated by spillover, and would therefore seem to waste postsynaptic resources.

5.8 Model for synapse enlargement during LTP

The results of this study suggest the following model for synapse enlargement that occurs following LTP induction (Figure 5.1). TBS-induced LTP stimulates release of glutamate from the presynaptic axon and recruitment of additional DCVs to existing presynaptic active zones, which transport crucial active zone proteins. The dense cores are likely to include CAMs, specifically cadherins, which localize in puncta at the edges of mature synapses (i.e. VFTZs), and neurexins and ephrins, which signal their postsynaptic partners to initiate synaptogenesis. Once DCVs are inserted into the presynaptic membrane to enlarge the presynaptic active zone, the CAMs that occupy their cores signal across the cleft and recruit their postsynaptic partners. The bidirectional signaling between these CAMs induces mobilization of additional NMDARs, AMPARs, PSD-95, and other postsynaptic proteins, as well as presynaptic vesicles. At the same time, enhanced glutamate release from the presynaptic cell increases postsynaptic NMDA receptor response. This increased activity recruits even more additional AMPA receptors from the perisynatic region (supplied by the extrasynaptic region, which is repopulated with AMPA receptors by exocytosis on dendrites) to enhance the postsynaptic response. Together these postsynaptic proteins, and others that are recruited from the cytoplasm and by additional protein synthesis cascades, create additional VFTZs. With the addition of VFTZs, synapses possess greater postsynaptic area populated by glutamate receptors that can respond to presynaptic glutamate release spillover from the synaptic active zone. At the same time, the presynaptic fusion pore diameter increases, allowing for rapid release of more glutamate into the cleft and greater activation of AMPARs within the synaptic active zone and in VFTZs. As VFTZs are created at potentiated synapses, VFTZs are reduced at unpotentiated synapses, as

functional AMPA modules are redistributed to enlarging synapses from their unpotentiated neighbors. All of these processes occur in a coordinated and homeostatic way. PSD enlargement that occurs at 2 hours following LTP induction is perfectly balanced by a reduction in spine number. The spines that have the largest increase in synapse area recruit more of the pre- and postsynaptic resources necessary for enlargement. This PSD enlargement is a result of VFTZ growth at 2 hours following LTP, which occurs by the balanced transfer of AMPA functional modules from unpotentiated to potentiated synapses, and enhances response at enlarged synapses following LTP induction.

References

Adesnick A, Nicoll RA, England PM (2005) Photoinactivation of native AMPA receptors reveals their real-time trafficking. Neuron 48(6):977-85.

Adams CL, Chen YT, Smith SJ, Nelson WJ (1998) Mechanisms of epithelial cell-cell adhesion and cell compaction revealed by high-resolution tracking of E-cadherin-green fluorescent protein. J Cell Biol 142:1105-1119.

Ahmari SE, Smith SJ (2002) Knowing a nascent synapse when you see it. Neuron 34:333-336.

Akins MR, Biederer T (2006) Cell-cell interactions in synaptogenesis. Curr Opin Neurobiol 16:83-89.

Ashby MC, De La Rue SA, Ralph GS, Uney J, Collingridge GL, Henley JM (2004) Removal of AMPA receptors (AMPARs) from synapses is preceded by transient endocytosis of extrasynaptic AMPARs. J Neurosci 24:5172-5176.

Ashby MC, Maier SR, Nishimune N, Henley JM (2006) Lateral Diffusion Drives Constitutive Exchange of AMPA Receptors at Dendritic Spines and Is Regulated by Spine Morphology. J Neurosci 26:7046-7055.

Bamji SX, Shimazu K, Kimes N, Huelsken J, Birchmeier W, Lu B, Reichardt LF (2003) Role of beta-catenin in synaptic vesicle localization and presynaptic assembly. Neuron 40:719-731.

Bats C, Groc L, Choquet D (2007) The interaction between stargazin and PSD-95 regulates AMPA receptor surface trafficking. Neuron 53:719 –734.

Beattie EC, Carroll RC, Yu X, Morishita W, Yasuda H, von Zastrow M, Malenka RC (2000) Regulation of AMPA receptor endocytosis by a signaling mechanism shared with LTD. Nat Neurosci 3:1291-1300.

Benson DL, Colman DR, Huntley GW (2001) Molecules, maps and synapse specificity. Nat Rev Neurosci 2:899-909.

Benson DL, Tanaka H (1998) N-cadherin redistribution during synaptogenesis in hippocampal neurons. J Neurosci 18:6892-6904.

Bliss TV, Collingridge GL (1993) A synaptic model of memory: long-term potentiation in the hippocampus. Nature 361:31-39.

Bolshakov VY, Siegelbaum SA (1995) Regulation of hippocampal transmitter release during development and long-term potentiation. Science 269:1730-1734.

Borgdorff AJ, Choquet D (2002) Regulation of AMPA receptor lateral movements. Nature 417:649-653.

Bourne JN, Harris KM (2008) Balancing structure and function at hippocampal dendritic spines. Annu Rev Neurosci 31:47-67.

Bourne JN, Harris KM (2011a) Coordination of size and number of excitatory and inhibitory synapses results in a balanced structural plasticity along mature hippocampal CA1 dendrites during LTP. Hippocampus 21:354-373.

Bourne JN, Harris KM (2011b) Smooth endoplasmic reticulum scales with synapse size and number along mature CA1 dendrites during long-term potentiation.

Bourne JN, Sorra KE, Hurlburt J, Harris KM (2007) Polyribosomes are increased in spines of CA1 dendrites 2 h after the induction of LTP in mature rat hippocampal slices. Hippocampus 17:1-4.

Bouwman J, Maia AS, Camoletto PG, Posthuma G, Roubos EW, Oorschot VM, Klumperman J, Verhage M (2004) Quantification of synapse formation and maintenance *in vivo* in the absence of synaptic release. Neurosci 126:115-126.

Bozdagi O, Valcin M, Poskanzer K, Tanaka H, Benson DL (2004) Temporally distinct demands for classic cadherins in synapse formation and maturation. Mol Cell Neurosci 27:509-521.

Bredt DS, Nicoll RA (2003) AMPA receptor trafficking at excitatory synapses. Neuron 40:361-379.

Bresler T, Ramati Y, Zamorano PL, Zhai R, Garner CC, Ziv NE (2001) The dynamics of SAP90/PSD-95 recruitment to new synaptic junctions. Mol Cell Neurosci 18:149-167.

Bresler T, Shapira M, Boeckers T, Dresbach T, Futter M, Garner CC, Rosenblum K, Gundelfinger ED, Ziv NE (2004) Postsynaptic density assembly is fundamentally different from presynaptic active zone assembly. J Neurosci 24:1507-1520.

Burns ME, Beushausen SA, Chin GJ, Tang D, DeBello WM, Dresbach T, OConnor V, Schweizer FE, Wang SSH, Whiteheart SW, Hawkey LA, Betz H, Augustine GJ (1995) Proteins involved in synaptic vesicle docking and fusion. Cld Spr Harbor Symp Quant Biol 60:337-348.

Carroll RC, Beattie EC, Xia H, Luscher C, Altschuler Y, Nicoll RA, Malenka RC, Von ZM (1999) Dynamin-dependent endocytosis of ionotropic glutamate receptors. Proc Natl Acad Sci U S A 96:14112-14117.

Cases-Langhoff C, Voss B, Garner AM, Appeltauer U, Takei K, Kindler S, Veh RW, De CP, Gundelfinger ED, Garner CC (1996) Piccolo, a novel 420 kDa protein associated with the presynaptic cytomatrix. Eur J Cell Biol 69:214-223.

Chavis P, Westbrook G (2001) Integrins mediate functional pre- and postsynaptic maturation at a hippocampal synapse. Nature 411:317-321.

Chirillo, MA et al. (2009) Presynaptic Structural Plasticity Following the Induction of LTP in Hippocampal Area CA1 of the Mature Rat. Poster number 620.13. *Society for Neuroscience,* 2009: Chicago, IL.

Choi S, Klingauf J, Tsien RW (2000) Postfusional regulation of cleft glutamate concentration during LTP at 'silent synapses'. Nat Neurosci. 3:330–336.

Chubykin AA, Atasoy D, Etherton MR, Brose N, Kavalali ET, Gibson JR, Sudhof TC (2007) Activity-dependent validation of excitatory versus inhibitory synapses by neuroligin-1 versus neuroligin-2. Neuron 54:919-931.

Collin C, Miyaguchi K, Segal M (1997) Dendritic spine density and LTP induction in cultured hippocampal slices. J Neurophysiol 77:1614-1623.

Collingridge GL, Isaac JT, Wang YT (2004) Receptor trafficking and synaptic plasticity. Nat Rev Neurosci 5:952-962.

Cooney JR, Hurlburt JL, Selig DK, Harris KM, Fiala JC (2002) Endosomal Compartments Serve Multiple Hippocampal Dendritic Spines from a Widespread Rather Than a Local Store of Recycling Membrane. J Neurosci *22*(6):2215–2224.

Cotman C, Taylor D, Lynch G (1973) Ultrastructural changes in synapses in the dentate gyrus of the rat during development. Brain Res 63:205-213.

Cotman C, Taylor D (1972) Isolation and structural studies on synaptic complexes from rat brain. Journal of Cell Biology 55:696-711.

Craig AM, Blackstone CD, Huganir RL, Banker G (1994) Selective clustering of glutamate and gamma-aminobutyric acid receptors opposite terminals releasing the corresponding neurotransmitters. Proc Natl Acad Sci U S A 91:12373-12377.

Dai Z, Peng HB (1996) Dynamics of synaptic vesicles in cultured spinal cord neurons in relationship to synaptogenesis. Mol Cell Neurosci 7:443-452.

Dailey ME, Smith SJ (1996) The dynamics of dendritic structure in developing hippocampal slices. J Neurosci 16:2983-2994.

Dalva MB, Takasu MA, Lin MZ, Shamah SM, Hu L, Gale NW, Greenberg ME (2000) EphB receptors interact with NMDA receptors and regulate excitatory synapse formation. Cell 103:945-956.

Daniels DL, Eklof Spink K, Weis WI (2001) Beta-catenin: molecular plasticity and drug design. Trends Biochem. Sci. 26:672–78

de WJ, Sylwestrak E, O'Sullivan ML, Otto S, Tiglio K, Savas JN, Yates JR, III, Comoletti D, Taylor P, Ghosh A (2009) LRRTM2 interacts with Neurexin1 and regulates excitatory synapse formation. Neuron 64:799-806.

Dean C, Scholl FG, Choih J, DeMaria S, Berger J, Isacoff E, Scheiffele P (2003) Neurexin mediates the assembly of presynaptic terminals. Nat Neurosci 6:708-716.

Desmond NL, Levy WB (1983) Synaptic correlates of associative potentiation/depression: an ultrastructural study in the hippocampus. Brain Res 265:21-30.

Desmond NL, Levy WB (1986a) Changes in the numerical density of synaptic contacts with long-term potentiation in the hippocampal dentate gyrus. J Comp Neurol 253:466-475.

Desmond NL, Levy WB (1986b) Changes in the postsynaptic density with long-term potentiation in the dentate gyrus. J Comp Neurol 253:476-482.

Dityatev A, Dityateva G, Sytnyk V, Delling M, Toni N, Nikonenko I, Muller D, Schachner M (2004) Polysialylated neural cell adhesion molecule promotes remodeling and formation of hippocampal synapses. J Neurosci 24:9372-9382.

Durand GM, Kovalchuk Y, Konnerth A (1996) Long-term potentiation and functional synapse induction in developing hippocampus. Nature 381:71–75.

Ehlers MD (2000) Reinsertion or degradation of AMPA receptors determined by activity-dependent endocytic sorting. Neuron 28:511-525.

Ehlers MD, Heine M, Groc L, Lee MC,Choquet D (2007) Diffusional Trapping of GluR1 AMPA Receptors by Input-Specific Synaptic Activity. Neuron 54:447-460.

Elste AM, Benson DL (2006) Structural basis for developmentally regulated changes in cadherin function at synapses. J Comp Neurol 495:324-335.

Fedor, P., BenÏ usÏkovaÂ , L., JakesÏ , H. and MajernõÂk, V., An L. BenÏ usÏkovaÂ / Neuroscience Letters 280 (2000) Dependence of magnitudes of electrophoretic velocity veff of postsynaptic vesicles and intensity of the intra-spine electric electrophoretic coupling mechanism between ef®ciency modi®cation of spine synapses and their stimulation. Studia Biophysica, 92 (1982) 141±146)

Fiala JC (2005) Reconstruct: a free editor for serial section microscopy. J Microsc 218:52-61.

Fiala JC, Harris KM (2001) Extending unbiased stereology of brain ultrastructure to three- dimensional volumes. J Am Med Inform Assoc 8:1-16.

Fifkova E, Anderson CL (1981) Stimulation-induced changes in dimensions of stalks of dendritic spines in the dentate molecular layer. Exp Neurol 74:621-627.

Fifkova E, Van Harreveld A (1977) Long-lasting morphological changes in dendritic spines of dentate granular cells following stimulation of the entorhinal area. J Neurocytol 6:211-230.

Fischer M, Kaech S, Wagner U, Brinkhaus H, Matus A (2000) Glutamate receptors regulate actin-based plasticity in dendritic spines. Nat Neurosci 3:887-894.

Franks KM, Bartol TM Jr., Sejnowski TJ (2002) A Monte Carlo model reveals independent signaling at central glutamatergic synapses. J Biophys. 83:2333–2348.

Friedman HV, Bresler T, Garner CC, Ziv NE (2000) Assembly of new individual excitatory synapses: time course and temporal order of synaptic molecule recruitment. Neuron 27:57-69.

Garner CC, Kindler S, Gundelfinger ED (2000) Molecular determinants of presynaptic active zones. Curr Opin Neurobiol 10:321-327.

Geinisman Y, de Toledo-Morrell L, Morrell F, Heller RE, Rossi M, Parshall RF (1993) Structural synaptic correlate of long-term potentiation: formation of axospinous synapses with multiple, completely partitioned transmission zones. Hippocampus 3:435-445.

Geinisman Y, Toledo-Morrell L, Morrell F (1991) Induction of long-term potentiation is associated with an increase in the number of axospinous synapses with segmented postsynaptic densities. Brain Res 566:77-88.

Gerrow K, Romorini S, Nabi SM, Colicos MA, Sala C, El-Husseini A (2006) A preformed complex of postsynaptic proteins is involved in excitatory synapse development. Neuron 49:547-562.

Graf ER, Zhang X, Jin SX, Linhoff MW, Craig AM (2004) Neurexins induce differentiation of GABA and glutamate postsynaptic specializations via neuroligins. Cell 119:1013-1026.

Groc L, Heine M, Cognet L, Brickley K, Stephenson FA, Lounis B, Choquet D (2004) Differential activity-dependent regulation of the lateral mobilities of AMPA and NMDA receptors. Nat Neurosci 7:695-696.

Harms KJ, Craig AM (2005) Synapse composition and organization following chronic activity blockade in cultured hippocampal neurons. J Comp Neurol 490:72-84.

Harris KM, Jensen FE, Tsao B (1992) Three-dimensional structure of dendritic spines and synapses in rat hippocampus (CA1) at postnatal day 15 and adult ages: implications for the maturation of synaptic physiology and long-term potentiation. J Neurosci 12:2685-2705.

Harris KM, Kater SB (1994) Dendritic spines: cellular specializations imparting both stability and flexibility to synaptic function. Annu Rev Neurosci 17:341-371.

Harris KM, Perry E, Bourne J, Feinberg M, Ostroff L, Hurlburt J (2006) Uniform serial sectioning for transmission electron microscopy. J Neurosci 26:12101-12103.

Harris KM, Stevens JK (1988) The development of long-term potentiation in hippocampus and neocortex. Neuropsychologia. 27:31-39.

Harris KM, Stevens JK (1989) Dendritic spines of CA1 pyramidal cells in the rat hippocampus: serial electron microscopy with reference to their biophysical characteristics. J Neurosci 9:2982-2997.

Hayashi Y, Shi SH, Esteban JA, Piccini A, Poncer JC, Malinow R (2000) Driving AMPA receptors into synapses by LTP and CaMKII: requirement for GluR1 and PDZ domain interaction. Science 287:2262-2267.

Henkemeyer M, Itkis OS, Ngo M, Hickmott PW, Ethell IM (2003) Multiple EphB receptor tyrosine kinases shape dendritic spines in the hippocampus. J Cell Biol 163:1313-1326.

Hering H, Sheng M (2001) Dendritic spines: structure, dynamics and regulation. Nat Rev Neurosci 2:880-888.

Hollmann M, Heinemann S (1994) Cloned glutamate receptors. Annu Rev Neurosci 17:31-108.

Huntley GW, Elste AM, Patil SB, Bozdagi O, Benson DL, Steward O (2012) Synaptic Loss and Retention of Different Classic Cadherins With LTP-Associated Synaptic Structural Remodeling *In Vivo*. Hippocampus 22:17-28.

Ichtchenko K, Hata Y, Nguyen T, Ullrich B, Missler M, Moomaw C, Sudhof TC (1995) Neuroligin 1: a splice site-specific ligand for beta-neurexins. Cell 81:435-443.

Irie M, Hata Y, Takeuchi M, Ichtchenko K, Toyoda A, Hirao K, Takai Y, Rosahl TW, Sudhof TC (1997) Binding of neuroligins to PSD-95. Science 277:1511-1515.

Isaac JT, Ashby MC, McBain CJ (2007) The role of the GluR2 subunit in AMPA receptor function and synaptic plasticity. Neuron 54:859-871.

Isaac JT, Nicoll RA, Malenka RC (1995) Evidence for silent synapses: implications for the expression of LTP. Neuron 15:427–434.

Ivanov D, Philippova M, Antropova J, Gubaeva F, Iljinskaya O, Tararak E, Bochkov V, Erne P, Resink T, Tkachuk V (2001) Expression of cell adhesion molecule T-cadherin in the human vasculature. Histochem Cell Biol 115:231-242.

Jack JJ, Larkman AU, Major G, Stratford KJ (1994) Quantal analysis of the synaptic excitation of CA1 hippocampal pyramidal cells. In: Molecular and Cellular Mechanisms of Neurotransmitter Release (Stjarne L, Greengard P, Grillner S, Hokfelt T, Ottoson D, eds), New York: Raven Press, Ltd.

Jensen FE, Harris KM (1989) Preservation of neuronal ultrastructure in hippocampal slices using rapid microwave-enhanced fixation. J Neurosci Methods 29:217-230.

Jontes JD, Emond MR, Smith SJ (2004) *In vivo* trafficking and targeting of N-cadherin to nascent presynaptic terminals. J Neurosci 24:9027-9034.

Kayser MS, McClelland AC, Hughes EG, Dalva MB (2006) Intracellular and trans-synaptic regulation of glutamatergic synaptogenesis by EphB receptors. J Neurosci 26:12152-12164.

Kennedy MB (2000) Signal-processing machines at the postsynaptic density. Science 290:750-754.

Kennedy MJ, Davison IG, Robinson CG, Ehlers MD (2010) Syntaxin-4 defines a domain for activity-dependent exocytosis in dendritic spines. Cell 141:524–535.

Khaing ZZ, Fidler L, Nandy N, Phillips GR (2006) Structural stabilization of CNS synapses during postnatal development in rat cortex. J Neurochem 98(2):471-80.

Kharazia VN, Phend KD, Rustioni A, Weinberg RJ (1996) EM colocalization of AMPA and NMDA receptor subunits at synapses in rat cerebral cortex. Neurosci Lett 210:37-40.

Ko J, Zhang C, Arac D, Boucard AA, Brunger AT, Su¨dhof TC (2009) Neuroligin-1 performs neurexin-dependent and neurexin-independent functions in synapse validation. EMBO J 28:3244 –3255.

Kornau HC, Schenker LT, Kennedy MB, Seeburg PH (1995) Domain interaction between NMDA receptor subunits and the postsynaptic density protein PSD-95. Science 269:1737-1740.

Lang C, Barco A, Zablow L, Kandel ER, Siegelbaum SA, Zakharenko SS (2004) Transient expansion of synaptically connected dendritic spines upon induction of hippocampal long-term potentiation. Proc Natl Acad Sci U S A 101:16665-16670.

Lavenex P, Lavenex PB, Bennett JL, Amaral DG (2009) Postmortem changes in the neuroanatomical characteristics of the primate brain: hippocampal formation. J Comp Neurol 512:27-51.

Levinson JN, Chery N, Huang K, Wong TP, Gerrow K, Kang R, Prange O, Wang YT, El Husseini A (2005) Neuroligins mediate excitatory and inhibitory synapse formation: involvement of PSD-95 and neurexin-1beta in neuroligin-induced synaptic specificity. J Biol Chem 280:17312–17319.

Li P, Kerchner GA, Sala C, Wei F, Huettner JE, Sheng M, Zhuo M (1999) AMPA receptor-PDZ interactions in facilitation of spinal sensory synapses. Nat Neurosci 2:972-977.

Li Z, Sheng M (2003) Some assembly required: the development of neuronal synapses. Nat Rev Mol Cell Biol 4:833-841.

Liao D, Hessler NA, Malinow R (1995) Activation of postsynaptically silent synapses during pairing-induced LTP in CA1 region of hippocampal slice. Nature 375:400–404.

Liao D, Zhang X, O'Brien R, Ehlers MD, Huganir RL (1999) Regulation of morphological postsynaptic silent synapses in developing hippocampal neurons. Nat Neurosci 2:37–43.

Lin DT, Makino Y, Sharma K, Hayashi T, Neve R, Takamiya K, Huganir RL (2009) Regulation of AMPA receptor extrasynaptic insertion by 4.1 N, phosphorylation and palmitoylation. Nat Neurosci 12:879–887.

Linhoff MW, Lauren J, Cassidy RM, Dobie FA, Takahashi H, Nygaard HB, Airaksinen MS, Strittmatter SM, Craig AM (2009) An unbiased expression screen for synaptogenic proteins identifies the LRRTM protein family as synaptic organizers. Neuron 61:734-749.

Lisman J, Harris KM (1993) Quantal analysis and synaptic anatomy - integrating two views of hippocampal plasticity. Trends Neurosci 16:141-147.

Lisman J, Raghavachari S (2006) A unified model of the presynaptic and postsynaptic changes during LTP at CA1 synapses. Science's STKE [online] http://stke.sciencemag.org/cgi/content/full/sigtrans;2006/356/re11.

Lissin DV, Carroll RC, Nicoll RA, Malenka RC, Von ZM (1999) Rapid, activation-induced redistribution of ionotropic glutamate receptors in cultured hippocampal neurons. J Neurosci 19:1263-1272.

Liu G, Tsien RW (1995) Properties of synaptic transmission at single hippocampal synaptic boutons. Nature 375:404-408.

Liu G, Choi S, Tsien RW (1999) Variability of neurotransmitter concentration and nonsaturation of postsynaptic AMPA receptors at synapses in hippocampal cultures and slices. Neuron 22:395–409.

Lledo PM, Hjelmstad GO, Mukherji S, Soderling TR, Malenka RC, Nicoll RA (1995) Calcium calmodulin-dependent kinase-II and long term potentiation enhance synaptic transmission by the same mechanism. Proc Natl Acad Sci USA 92:11175-11179.

Lohmann C, Finski A, Bonhoeffer T (2005) Local calcium transients regulate the spontaneous motility of dendritic filopodia. Nat Neurosci 8:305-312.

Lu W, Man H, Ju W, Trimble WS, MacDonald JF, Wang YT (2001) Activation of synaptic NMDA receptors induces membrane insertion of new AMPA receptors and LTP in cultured hippocampal neurons. Neuron 29:243-254.

Luscher C, Nicoll RA, Malenka RC, Muller D (2000) Synaptic plasticity and dynamic modulation of the postsynaptic membrane. Nat Neurosci 3:545-550.

Luscher C, Xia H, Beattie EC, Carroll RC, von Zastrow M, Malenka RC, Nicoll RA (1999) Role of AMPA receptor cycling in synaptic transmission and plasticity. Neuron 24:649-658.

Magee JC, Cook EP (2000) Somatic EPSP amplitude is independent of synapse location in hippocampal pyramidal neurons. Nat Neurosci. 3:895–903.

Makino H, Malinow R (2009) AMPA receptor incorporation into synapses during LTP: the role of lateral movement and exocytosis. Neuron 64:381-390.

Malenka RC (2003) Synaptic plasticity and AMPA receptor trafficking. Ann N Y Acad Sci 1003:1-11.

Malinow R, Malenka RC (2002) AMPA receptor trafficking and synaptic plasticity. Annu Rev Neurosci 25:103-126.

Man HY, Lin JW, Ju WH, Ahmadian G, Liu L, Becker LE, Sheng M, Wang YT (2000) Regulation of AMPA receptor-mediated synaptic transmission by clathrin-dependent receptor internalization. Neuron 25:649-662.

Marrs GS, Green SH, Dailey ME (2001) Rapid formation and remodeling of postsynaptic densities in developing dendrites. Nat Neurosci 4:1006-1013.

Masugi-Tokita M, Tarusawa E, Watanabe M, Molnar E, Fujimoto K, Shigemoto R (2007) Number and density of AMPA receptors in individual synapses in the rat cerebellum as revealed by SDS-digested freeze-fracture replica labeling. J Neurosci 27:2135-2144.

Matsuzaki M, Ellis-Davies GC, Nemoto T, Miyashita Y, Iino M, Kasai H (2001) Dendritic spine geometry is critical for AMPA receptor expression in hippocampal CA1 pyramidal neurons. Nat Neurosci 4:1086-1092.

Matsuzaki M, Honkura N, Ellis-Davies GC, Kasai H (2004) Structural basis of long-term potentiation in single dendritic spines. Nature 429:761-766.

McAllister AK, Stevens CF (2000) Nonsaturation of AMPA and NMDA receptors at hippocampal synapses. Proc. Natl Acad. Sci. USA 97:6173–6178.

McAllister AK (2007) Dynamic Aspects of CNS synapse formation. Annu Rev Neurosci 30:425-50.

McKinney RA, Capogna M, Durr R, Gahwiler BH, Thompson SM (1999) Miniature synaptic events maintain dendritic spines via AMPA receptor activation. Nat Neurosci 2:44-49.

Miller DC (1998) Use of perfusion fixation for improved neuropathologic examination. Arch Pathol Lab Med 122:949.

Missler M, Zhang W, Rohlmann A, Kattenstroth G, Hammer RE, Gottmann K, Sdhof TC (2003) Alpha-neurexins couple Ca2_ channels to synaptic vesicle exocytosis. Nature 423:939 –948.

Mohrmann R, Lessmann V, Gottmann K (2003) Developmental maturation of synaptic vesicle cycling as a distinctive feature of central glutamatergic synapses. Neurosci 117:7-18.

Mondin M, Labrousse V, Hosy E, Heine M, Tessier B, Levet F, Poujol C, Blanchet C, Choquet D, Thoumine O (2011) Neurexin-Neuroligin Adhesions Capture Surface-Diffusing AMPA Receptors through PSD-95 Scaffolds. J Neurosci 31:13500-13515.

Mukherjee K, Sharma M, Urlaub H, Bourenkov GP, Jahn R, Sudhof TC, Wahl MC (2008) CASK Functions as a Mg 2_-independent neurexin kinase.Cell 133:328 –339.

Nagerl UV, Eberhorn N, Cambridge SB, Bonhoeffer T (2004) Bidirectional activity-dependent morphological plasticity in hippocampal neurons. Neuron 44:759-767.

Nielsen TA, DiGregorio DA, Silver RA (2004) Modulation of glutamate mobility reveals the mechanism underlying slow-rising AMPAR EPSCs and the diffusion coefficient in the synaptic cleft. Neuron 42:757–771.

Nuriya M, Huganir RL (2006) Regulation of AMPA receptor trafficking by N-cadherin. J Neurochem 97:652-661.

Nusser Z (2000) AMPA and NMDA receptors: similarities and differences in their synaptic distribution. Curr Opin Neurobiol 10:337–341.

Ohtsuka T, Takao-Rikitsu E, Inoue E, Inoue M, Takeuchi M, Matsubara K, Deguchi-Tawarada M, Satoh K, Morimoto K, Nakanishi H, Takai Y (2002) Cast: a novel protein of the cytomatrix at the active zone of synapses that forms a ternary complex with RIM1 and munc13-1. J Cell Biol 158:577-590.

Okabe S, Kim HD, Miwa A, Kuriu T, Okado H (1999) Continual remodeling of postsynaptic density and its regulation by synaptic activity. Nat Neurosci 2:804-811.

Opazo P, Labrecque S, Tigaret CM, Frouin A, Wiseman PW, De Koninck P, Choquet D (2010) CaMKII triggers the diffusional trapping of surface AMPARs through phosphorylation of stargazin. Neuron 67:239 –252.

Ostroff LE, Fiala JC, Allwardt B, Harris KM (2002) Polyribosomes redistribute from dendritic shafts into spines with enlarged synapses during LTP in developing rat hippocampal slices. Neuron 35:535-545.

Papa M, Bundman MC, Greenberger V, Segal M (1995) Morphological analysis of dendritic spine development in primary cultures of hippocampal neurons. J Neurosci 15:1-11.

Park M, Salgado JM, Ostroff L, Helton TD, Robinson CG, Harris KM, Ehlers MD (2006) Plasticity-Induced Growth of Dendritic Spines by Exocytic Trafficking from Recycling Endosomes. Neuro 52(5):817-830.

Passafaro M, Piech V, Sheng M (2001) Subunit-specific temporal and spatial patterns of AMPA receptor exocytosis in hippocampal neurons. Nat Neurosci 4:917–926.

Pfenninger KH (1971) The cytochemistry of synaptic densities. I. An analysis of the bismuth lodide impregnation method. J Ultrastruct Res 34(1):103-22.

Passafaro M, Nakagawa T, Sala C, Sheng M (2003) Induction of dendritic spines by an extracellular domain of AMPA receptor subunit GluR2. Nature 424:677-681.

Petralia RS, Esteban JA, Wang YX, Partridge JG, Zhao HM, Wenthold RJ, Malinow R (1999) Selective acquisition of AMPA receptors over postnatal development suggests a molecular basis for silent synapses. Nat Neurosci 2:31–36.

Phillips GR, Huang JK, Wang Y, Tanaka H, Shapiro L, Zhang W, Shan WS, Arndt K, Frank M, Gordon RE, Gawinowicz MA, Zhao Y, Colman DR (2001) The presynaptic particle web: ultrastructure, composition, dissolution, and reconstitution. Neuron 32:63-77.

Pokorny J, Yamamoto T (1981) Postnatal ontogenesis of hippocampal CA1 area in rats. II. Development of ultrastructure in stratum lacunosum and moleculare. Brain Res Bull 7:121-130.

Popov VI, Davies HA, Rogachevsky VV, Patrushev IV, Errington ML, Gabbott PL, Bliss TV, Stewart MG (2004) Remodelling of synaptic morphology but unchanged synaptic density during late phase long-term potentiation (LTP): a serial section electron micrograph study in the dentate gyrus in the anaesthetised rat. Neurosci 128:251-262.

Purpura DP (1975) Dendritic differentiation in human cerebral cortex: Normal and aberrant developmental patterns. In: Advances in Neurology: Physiology and pathology of dendrites (Kreutzberg GW, ed), pp 91-116. New York, NY: Raven Press.

Raghavachari S, Lisman JE (2004) Properties of quantal transmission at CA1 synapses. J. Neurophysiol. 92:2456–2467.

Rao A, Kim E, Sheng M, Craig AM (1998) Heterogeneity in the molecular composition of excitatory postsynaptic sites during development of hippocampal neurons in culture. J Neurosci 18:1217-1229.

Roberts JC, McCrossan MV, Jones HB (1990) The case for perfusion fixation of large tissue samples for ultrastructural pathology. Ultrastruct Pathol 14:177-191.

Sabo SL, Gomes RA, McAllister AK (2006) Formation of presynaptic terminals at predefined sites along axons. J Neurosci 26:10813-10825.

Saglietti L, Dequidt C, Kamieniarz K, Rousset MC, Valnegri P, Thoumine O, Beretta F, Fagni L, Choquet D, Sala C, Sheng M, Passafaro M (2007) Extracellular interactions between GluR2 and N-cadherin in spine regulation. Neuron 54:461-477.

Sans N, Petralia RS, Wang YX, Blahos J, Hell JW, Wenthold RJ (2000) A developmental change in NMDA receptor-associated proteins at hippocampal synapses. J Neurosci 20:1260-1271.

Sans N, Prybylowski K, Petralia RS, Chang K, Wang YX, Racca C, Vicini S, Wenthold RJ (2003) NMDA receptor trafficking through an interaction between PDZ proteins and the exocyst complex. Nat Cell Biol 5:520-530.

Scheiffele P (2003) Cell-cell signaling during synapse formation in the CNS. Annu Rev Neurosci 26:485-508.

Schikorski T, Stevens CF (1997) Quantitative ultrastructural analysis of hippocampal excitatory synapses. J Neurosci 17:5858-5867.

Schwartz IR, Pappas GD, Purpura DP (1968) Fine Structure of Neurons and Synapses in Feline Hippocampus During Postnatal Ontogenesis. Experimental Neurology 22:394-&.

Shapira M, Zhai RG, Dresbach T, Bresler T, Torres VI, Gundelfinger ED, Ziv NE, Garner CC (2003) Unitary assembly of presynaptic active zones from Piccolo-Bassoon transport vesicles. Neuron 38:237-252.

Sharma K, Fong DK, Craig AM (2006) Postsynaptic protein mobility in dendritic spines: long-term regulation by synaptic NMDA receptor activation. Mol Cell Neurosci 31:702-712.

Sheng M, Kim MJ (2002) Postsynaptic signaling and plasticity mechanisms. Science 298:776-780.

Shepherd JD, Huganir RL (2007) The cell biology of synaptic plasticity: AMPA receptor trafficking. Annu Rev Cell Dev Biol 23:613-643.

Shi SH, Hayashi Y, Petralia RS, Zaman SH, Wenthold RJ, Svoboda K, Malinow R (1999) Rapid spine delivery and redistribution of AMPA receptors after synaptic NMDA receptor activation. Science 284:1811-1816.

Shi Y, Lu W, Milstein AD, Nicoll RA (2009) The stoichiometry of AMPA receptors and TARPs varies by neuronal cell type. Neuron 62:633– 640.

Siddiqui TJ, Pancaroglu R, Kang Y, Rooyakkers A, Craig AM (2010) LRRTMs and neuroligins bind neurexins with a differential code to cooperate in glutamate synapse development. J Neurosci 30:7495-7506.

Silver RA, Cull-Candy SG, Takahashi T (1996) Non-NMDA glutamate receptor occupancy and open probability at a rat cerebellar synapse with single and multiple release sites. J. Physiol. 494:231–250.

Silverman JB, Restituito S, Lu W, Lee-Edwards L, Khatri L, Ziff EB (2007) Synaptic anchorage of AMPA receptors by cadherins through neural plakophilin-related arm protein AMPA receptor-binding protein complexes. J Neurosci 27:8505-8516.

Snyder EM, Huber KM, Dong X, Fallon JR, Bear MF (2000) Group I metabotropic glutamate receptor activation initiates internalization of AMPA receptors in cultured hippocampal neurons. *Soc. Neurosci. Abstr* 134: 15.

Song I, Huganir RL (2002) Regulation of AMPA receptors during synaptic plasticity. Trends Neurosci 25:578-588.

Song JY, Ichtchenko K, Sudhof TC, Brose N (1999) Neuroligin-1 is a postsynaptic cell-adhesion molecule of excitatory synapses. Proc Natl Acad Sci U S A 96:1100-1105.

Sorra KE, Harris KM (1998) Stability in synapse number and size at 2 hr after long-term potentiation in hippocampal area CA1. J Neurosci 18:658-671.

Sorra KE, Mishra A, Kirov SA, Harris KM (2006) Dense core vesicles resemble active-zone transport vesicles and are diminished following synaptogenesis in mature hippocampal slices. Neurosci 141:2097-2106.

Spacek J, Harris KM (1997) Three-dimensional organization of smooth endoplasmic reticulum in hippocampal CA1 dendrites and dendritic spines of the immature and mature rat. J Neurosci 17:190-203.

Spacek J, Harris KM (1997) Three-dimensional organization of smooth endoplasmic reticulum in hippocampal CA1 dendrites and dendritic spines of the immature and mature rat. J Neurosci 17(1):190-203.

Spacek J, Harris KM (1998) Three-dimensional organization of cell adhesion junctions at synapses and dendritic spines in area CA1 of the rat hippocampus. J Comp Neurol 393:58-68.

Sudhof TC (2008) Neuroligins and neurexins link synaptic function to cognitive disease. Nature 455:903–911.

Svoboda K, Mainen ZF (1999) Synaptic [Ca2+]: intracellular stores spill their guts. Neuron 22:427-430.

Sytnyk V, Leshchyns'ka I, Dityatev A, Schachner M (2004) Trans-Golgi network delivery of synaptic proteins in synaptogenesis. J Cell Sci 117:381-388.

Tada T, Sheng M (2006) Molecular mechanisms of dendritic spine morphogenesis. Curr Opin Neurobiol 16:95-101.

Tanaka J, Matsuzaki M, Tarusawa E, Momiyama A, Molnar E, Kasai H, Shigemoto R (2005) Number and density of AMPA receptors in single synapses in immature cerebellum. J. Neurosci. 25:799–807.

Tardin C, Cognet L, Bats C, Lounis B, Choquet D (2003) Direct imaging of lateral movements of AMPA receptors inside synapses. EMBO J 22:4656-4665.

Tashiro A, Dunaevsky A, Blazeski R, Mason CA, Yuste R (2003) Bidirectional regulation of hippocampal mossy fiber filopodial motility by kainate receptors: a two-step model of synaptogenesis. Neuron 38:773-784.

Togashi H, Abe K, Mizoguchi A, Takaoka K, Chisaka O, Takeichi M (2002) Cadherin regulates dendritic spine morphogenesis. Neuron 35:77-89.

tom Dieck S, Sanmarti-Vila L, Langnaese K, Richter K, Kindler S, Soyke A, Wex H, Smalla KH, Kampf U, Franzer JT, Stumm M, Garner CC, Gundelfinger ED (1998) Bassoon, a novel zinc-finger CAG/glutamine-repeat protein selectively localized at the active zone of presynaptic nerve terminals. J Cell Biol 142:499-509.

Tovar KR, Westbrook GL (1999) The incorporation of NMDA receptors with a distinct subunit composition at nascent hippocampal synapses in vitro. J Neurosci 19:4180-4188.

Triller A, Choquet D (2005) Surface trafficking of receptors between synaptic and extrasynaptic membranes: and yet they do move! Trends Neurosci 28(3):133-139.

Trommald M, Hulleberg G, Andersen P (1996) Long-term potentiation is associated with new excitatory spine synapses on rat dentate granule cells. Learn Mem 3:218-228.

Trommald M, Vaaland JL, Blackstad TW, Andersen P (1990) Dendritic spine changes in rat dentate granule cells associated with long-term potentiation. In: Neurotoxicity of excitatory amino acids (Guidotti A, Costa E, eds), pp 163-174. New York: Raven Press, Ltd.

Uchida N, Honjo Y, Johnson KR, Wheelock MJ, Takeichi M (1996) The catenin/cadherin adhesion system is localized in synaptic junctions bordering transmitter release zones. J Cell Biol 135:767-779.

Varoqueaux F, Sigler A, Rhee JS, Brose N, Enk C, Reim K, Rosenmund C (2002) Total arrest of spontaneous and evoked synaptic transmission but normal synaptogenesis in the absence of Munc13-mediated vesicle priming. Proc Natl Acad Sci U S A 99:9037-9042.

Verhage M, Maia AS, Plomp JJ, Brussaard AB, Heeroma JH, Vermeer H, Toonen RF, Hammer RE, van den Berg TK, Missler M, Geuze HJ, Sudhof TC (2000) Synaptic

assembly of the brain in the absence of neurotransmitter secretion. Science 287:864-869.

Waites CL, Craig AM, Garner CC (2005) Mechanisms of vertebrate synaptogenesis. Annu Rev Neurosci 28:251-274.

Washbourne P, Bennett JE, McAllister AK (2002) Rapid recruitment of NMDA receptor transport packets to nascent synapses. Nat Neurosci 5:751-759.

Washbourne P, Liu XB, Jones EG, McAllister AK (2004) Cycling of NMDA receptors during trafficking in neurons before synapse formation. J Neurosci 24:8253-8264.

Yudowski GA, Puthenveedu MA, Leonoudakis D, Panicker S, Thorn KS, Beattie EC, von Zastrow M (2007) Real-time imaging of discrete exocytic events mediating surface delivery of AMPA receptors. J Neurosci 27:11112–11121.

Yuste R, Bonhoeffer T (2001) Morphological changes in dendritic spines associated with long-term synaptic plasticity. Annu Rev Neurosci 24:1071-1089.

Yuste R, Bonhoeffer T (2004) Genesis of dendritic spines: insights from ultrastructural and imaging studies. Nat Rev Neurosci 5:24-34.

Zhai R, Olias G, Chung WJ, Lester RA, tom DS, Langnaese K, Kreutz MR, Kindler S, Gundelfinger ED, Garner CC (2000) Temporal appearance of the presynaptic cytomatrix protein bassoon during synaptogenesis. Mol Cell Neurosci 15:417-428.

Zhai RG, Vardinon-Friedman H, Cases-Langhoff C, Becker B, Gundelfinger ED, Ziv NE, Garner CC (2001) Assembling the presynaptic active zone: a characterization of an active one precursor vesicle. Neuron 29:131-143.

Zhang W, Benson DL (2001) Stages of synapse development defined by dependence on F-actin. J Neurosci 21:5169-5181.

Zhang W, Benson DL (2002) Developmentally regulated changes in cellular compartmentation and synaptic distribution of actin in hippocampal neurons. J Neurosci Res 69:427-436.

Zhou Q, Xiao M, Nicoll RA (2001) Contribution of cytoskeleton to the internalization of AMPA receptors. Proc Natl Acad Sci U S A 98:1261-1266.

Zito K, Scheuss V, Knott G, Hill T, Svoboda K (2009) Functional Maturation of Nascent Dendritic Spines. Neuron 61:247:258.

Ziv NE, Garner CC (2004) Cellular and molecular mechanisms of presynaptic assembly. Nat Rev Neurosci 5:385-399.

Ziv NE, Smith SJ (1996) Evidence for a role of dendritic filopodia in synaptogenesis and spine formation. Neuron 17:91-102.